The UV Calibration of the Hubble Space Telescope. IV. Absolute IUE Fluxes of HST Standard Stars

R. C. Bohlin
Space Telescope Science Institute

A. W. Harris
Rutherford Appleton Laboratory

A. V. Holm
Computer Sciences Corporation

C. Gry
Laboratoire d'Astronomie Spatiale

Submitted to Ap. J. Suppl. 89 Jul 17

ABSTRACT

Absolute UV fluxes are presented for 37 stars selected as calibration standards for the *Hubble Space Telescope* (*HST*). In order to provide data of maximum precision, new absolute calibrations have been derived for the *International Ultraviolet Explorer* (*IUE*) SWP and LWR cameras for point sources in the large apertures, while the sensitivities of the trail and small aperture observing modes relative to the large apertures are updated for all three *IUE* cameras. More than 2700 individual spectra are used to define the absolute flux distributions of the 37 *HST* standard stars in the wavelength range 1150–3300 Å. A comparison with white dwarf model atmosphere calculations suggests that the systematic external errors in the fluxes are less than 15%, while comparison with *ANS* flux measurements demonstrates an internal consistency of the *IUE* spectrophotometry of 2%, over a dynamic range of 10^4, in bandpasses of 100 Å or greater. The *IUE* fluxes at the longest wavelengths agree with ground-based data to an accuracy of 3%.

I. INTRODUCTION

HST has five scientific instruments that are sensitive to UV light and require UV standard stars for their calibrations. The five are two spectrographs (the Goddard High Resolution Spectrograph GHRS and the Faint Object Spectrograph FOS), two cameras (the Faint Object Camera FOC and the Wide Field and Planetary Camera WFPC), and the High Speed Photometer (HSP). Both cameras have modes for obtaining low resolution UV spectra. The calibrations require standard UV sources for linearity checks, spectral flat fielding, and scattered light measurements, in addition to the main purpose of absolute sensitivity determination.

In this paper, the results of a long-term collaborative program of the Space Telescope Science Institute and the Villafranca *IUE* Observatory (VILSPA) are presented, in which selected *HST* calibration stars have been observed repeatedly in the low dispersion mode of *IUE*. Many of the brighter stars in the program are well represented in the *IUE* data-bank, and de-archived spectra alone have satisfied our requirements in these cases. However, since the bright limit of the FOC slit spectrograph is about $V = 15$, high quality data are needed down to the faint limit of *IUE*'s observing capability (Boggess *et al.* 1978).

This Paper IV completes a series devoted to the calibration of the *HST* in the ultraviolet. The earlier papers I–III (Bohlin 1986; Bohlin and Grillmair 1988a,b) address the fundamental calibration of *IUE* and the corrections needed to achieve the stringent level of accuracy required by this program. The calibration corrections in Paper I are superseded by the results presented here in Paper IV.

II. HST STANDARD STAR SELECTION AND IUE OBSERVATIONS

The selection of standard stars for the *HST* is based on the following considerations:

1. A sufficiently large sample of stars is chosen, so that any star found to have small amplitude variability can be removed from the sample with minimal effect on the *HST* calibration.
2. Standard stars are distributed widely about the sky to minimize the average slewing time and to maximize the number of available calibration targets at any time of the year.
3. Stars of a variety of spectral types and with few prominent spectral features are chosen to reduce the chance that a particular absorption feature common to all the stars could lead to calibration errors at the corresponding wavelength.
4. Some high ecliptic latitude stars are included, since *HST* can observe the part of the sky that is near the orbital pole and more than 50° from the sun at any time of the year.
5. Some low latitude or southern stars are included to ensure that all ground-based observatories can see some *HST* standards.

Stars, such as HZ43, with close companions are rejected, because the flux contributed by the companion depends on the size of the entrance aperture.

The five prime *IUE* standards HD 60753, BD+75°325, HD 93521, BD+33°2642, and BD+28°4211 have been observed regularly by *IUE* throughout its operational history and have the most accurately determined spectra of all stars in the chosen sample. Therefore, these five stars are preferred for UV calibration work.

The observations obtained at the Goddard Space Flight Center (*GSFC*) were tailored to minimize the errors introduced by the detector artifacts. Two aspects of the detectors were considered: their low signal-to-noise and their non-linearities. Improvements in the signal-to-noise ratio, within the limitations of dynamic range and observing time, were made by increasing the area in the large apertures over which flux is collected. For stars brighter

than 11th magnitude and for G191-B2B, trailed exposures were performed in the standard way. For fainter stars, multiple exposures at different positions on the major axis of the aperture were a more effective way of improving the signal-to-noise. In general, only a small range of the spectrum was exposed optimally in each detector. Typically, the well exposed part of the spectrum was centered at 1300 Å in the SWP and at 2700–2800 Å in the LWP camera. To improve the signal-to-noise ratio for many of the stars in the parts of the spectra falling on the less sensitive areas of the detector, additional observations were obtained with deliberate overexposures of up to three times the optimum exposure. In these cases, good exposure levels at 1850 Å in the SWP and at 2200 Å in the LWP were the goal. Tests of linearity demonstrated that any errors introduced by the overexposures are less than 1.5% in broad bands.

Over a period of 6 years, observations of the faintest stars in the program, namely hot white dwarfs with (V = 14–15.5), have been made from the *VILSPA IUE* groundstation. In general, such stars can only be observed with *IUE* by means of the blind-offset technique (Harris and Sonneborn 1987), which requires coordinates accurate to 1 arcsec. Since white dwarfs generally have large proper motions, special care was necessary in determining positions. Accurate coordinate measurements of target and offset stars were made on new photographic plates provided by the Spanish Centro Astronomico de Yebes. Blind-offset maneuvers were monitored to ensure that the target star was centered in the spectrograph aperture as precisely as possible. Checks on the consistency of absolute flux levels were made by comparing spectra of the same star taken on different observing runs. In particular, some spectra of the stars HZ 21 and LDS 235B have anomalously low flux levels. In the case of HZ 21, the spectra in question are omitted from the final average spectrum. Due to the relatively long exposure times required for LDS 235B, the number of spectra obtained for this target is insufficient to dispel suspicions of variability; and LDS 235B is not in the present *HST* standard star list.

The selected *HST* standard stars are listed in Table 1. Columns 1 and 2 give the HD numbers and names of the stars. Columns 3 and 4 give right-ascension and declination coordinates for equinox 2000. The spectral type and photometric data in columns 5, 6, and 7 are mostly from Hoffleit (1964), Johnson *et al.* (1966), and Nicolet (1978) for the brighter stars and from McCook and Sion (1984) for the white dwarfs. Intrinsic colors used to compute E(B-V) in column 8 are from FitzGerald (1970). Further references are given in Turnshek *et al.* (1989). The numbers of *IUE* spectra averaged to produce the final data-set are given by *IUE* camera and observing mode (large aperture, trailed, small aperture plus multiple exposures in the large aperture) in columns 10, 11 and 12; and the grand total for each star is listed in column 13. Columns 14 and 15 give the average over wavelength of the standard deviation from the mean of the individual spectra for the short-wavelength (SWP) and long-wavelength (LW) spectra, respectively. The standard deviation from the mean is calculated for each point and then averaged over the intervals 1280–1970 Å for SWP and 1970–3200 Å for the LW data.

The set of UV standards consists of 34 hot stars and 3 additional cool stars for the measurement of scattered light from the gratings. The dynamic range of the UV fluxes is nearly 10^6, from η UMa (V = 1.86) to LDS 749B (V = 15.35).

III. COMPREHENSIVE RE-CALIBRATION OF IUE

a) History and Philosophy

An absolute flux calibration for *IUE* is applicable to the spectrum that is extracted from a linearized image from one of the SEC television cameras. An image is linearized by application of an Intensity Transfer Function (ITF) (Bohlin *et al.* 1980). For a brief description of *IUE*'s complement of cameras and their operational histories see Harris and Sonneborn (1987). *IUE* production processing applies absolute calibrations to low-dispersion spectra from all three cameras. The absolute calibrations of the SWP (for ITF2) and of the LWR (for ITF1) were completed in May 1980 by Bohlin and Holm (1980), republished by Holm *et al.* (1982), and modified in Paper I to correct errors. The May 1980 calibration is the only one that has been used for SWP and LWR routine production processing. The original absolute calibration used for the LWP (for ITF1) in production processing is that of Cassatella and Harris (1983). In 1984–5, the *IUE* project obtained data for new ITFs for all three cameras and an extensive set of new low dispersion spectra of *IUE* standard stars to provide absolute calibrations for the new ITFs. See Imhoff (1989) for a complete history of the ITFs. However, only the new LWP ITF (ITF2) and associated absolute calibration (Cassatella, Lloyd, and Riestra 1988) have been implemented to date in the routine *IUE* data processing. The new comprehensive set of *IUE* spectra of the *OAO 2* flux standards (Code and Meade 1979) provides a much improved basis for deriving a new calibration of the SWP ITF2 and LWR ITF1 data after the corrections described in Papers II and III have been applied to provide a time independent *IUE* data set. All SWP and LWR data used to define the fluxes for the *HST* standards are based on this re-calibration for SWP ITF2 and LWR ITF1. The planned reprocessing of the entire *IUE* archive will use absolute calibrations derived from these same *IUE* spectra of the *OAO 2* standards as processed with the new SWP ITF3 and LWR ITF2, or other suitable new ITFs. Consequently, the recalibration described here for SWP and LWR produces fluxes compatible with the final *IUE* archive and with current LWP fluxes.

b) Relative Sensitivity of the Low-dispersion Observing Modes

IUE absolute calibrations are for point source objects that are centered in the large entrance aperture (L). Since the small aperture (S) and the trailed (T) observing modes have different relative responses with wavelength (Harris and Cassatella 1985 and Paper I), the relative sensitivities S/L and T/L must be derived in order to optimize the accuracy of the *IUE* fluxes for the bright reference standards. Values of S/L and T/L for the SWP and LWR cameras were published in Paper I; and Bohlin (1988) revised T/L for the LWR. These ratios are computed for the LWP ITF1 and ITF2 and are presented in Table 2 along with those for the SWP and LWR, which are included for completeness. The values of T/L assume large aperture lengths of $21\farcs4$ and $20\farcs5$ for the SWP and LW spectrographs, respectively (Panek 1982). The S/L and T/L ratios are computed using hundreds of the spectra of the five *IUE* standard stars HD 60753, BD+75°325, HD 93521, BD+33°2642, and BD+28°4211 that are available in the *IUE* archive.

c) Absolute Re-calibration for SWP and LWR

The accuracy of the *IUE* spectrophotometric calibration depends on the precision of the absolute fluxes of the reference standards and on the fidelity of the transfer of the reference flux scale. The basis for the *IUE* reference flux scale is the flux specified for η UMa, which has an estimated accuracy of 10% (Bohlin *et al.* 1980). This fundamental choice provides a

correction to the *OAO 2* (Code and Meade 1979) and *TD-1* (Jamar *et al.* 1976) reference standards (Bohlin and Holm 1984). Originally in 1979–1980, the transfer of the reference flux scale to *IUE* was done with inadequate precision, because only a few *IUE* spectra of the bright *OAO 2* standards were available and because the early calibration techniques were primitive. Of fundamental importance to the re-calibration was the perfection of the high speed trail technique that is required to obtain photometric spectra of the brightest *OAO 2* stars (Oliversen 1986). The high speed trailed spectra, together with the many point source observations obtained in 1984–5, provide a vastly superior set of spectra of the six *OAO 2* standard stars (*i.e.* ζ Cas, η Aur, λ Lep, μ Col, η UMa, and 10 Lac) for the purpose of a comprehensive re-calibration.

After the change in sensitivity with time is corrected according to Papers II and III and after the S and T spectra are corrected to the large aperture relative response, all spectra can be used to define the large-aperture response. The corrections in time are normalized to unity in the first year of *IUE* operations, 1978.36–1979.36, so that the derived large-aperture calibration applies to the sensitivity in that period. The reference temperatures (THDA) of the calibrations are 8 C and 12 C for SWP and LWR, respectively. The calibration technique is detailed by Lindler and Bohlin (1986) and results in a smooth calibration defined every 5 Å. The new inverse sensitivities S^{-1} for the SWP and LWR large aperture in low dispersion are given in Table 3.

With respect to the Paper I calibration, the re-calibration gives fluxes which are generally lower by as much as 10%. The *IUE* calibration is specified on 5 Å centers in a smooth curve instead of the original 25 Å for SWP and 50 Å for LWR, because linear interpolation over 5 Å intervals in the smooth curve produces numerical errors that are well below 1%.

d) Absolute Calibration of the LWP

Since data reduced with both ITF1 and ITF2 for the LWP exist in the archive, a comparison of the fluxes from the two different ITFs is relevant. However, a direct comparison is complicated, because for any image only data processed with one ITF are available in the archive. Oliversen (1988) compared fluxes of 50 spectra processed with both ITFs and corresponding absolute calibrations and updated the absolute calibration of Cassatella and Harris (1983) in order to make the ITF1 fluxes consistent with those from ITF2. Since our ITF1 fluxes are based on a smoothed version of the Oliversen correction, the ITF1 and ITF2 fluxes should agree. For LWP spectra of the five *IUE* standard stars in the large aperture, a comparison between 295 spectra processed with ITF1 and 151 of those same spectra processed with ITF2 shows agreement to 1% from 2000 to 3100 Å when averaged over 100 Å wavelength bands (Figure 1). The structure of the apparent noise in Figure 1 is nearly identical in all five of the independent ratios and is caused by fixed pattern noise from the processing of these spectra, which all have low background and optimal exposure levels.

A comparison of LWP ITF1 fluxes with LWR fluxes is also made. Using a total of 479 LWP spectra and 625 LWR spectra of the 5 *IUE* standard stars, Figure 2 shows that the LWP fluxes are lower than those from the LWR by about 2% in the 2100–2400 Å range and higher by 2% between 2500 and 2900 Å. These ratios of LWP/LWR are consistent for all 5 stars. Since the time change of LWP sensitivity is a few per cent over the relevant time interval (1982.0–1987.0), a correction for this effect is needed before investigating these small discrepancies further. The systematic internal error of the LW fluxes of $\pm$ 1% about their average is small in comparison with the systematic external uncertainty of $\pm$ 10%.

IV. THE FLUXES

The *IUE* spectra in this work are extracted with the standard *IUE* production processing software. Systematic errors in the extracted spectra due to the original SWP ITF error, inaccurate wavelength assignments, temperature dependent camera sensitivity, and the camera high-voltage rise time, are corrected as described in Paper I. To get final flux distributions, the S/L, T/L, and time-dependent corrections are applied along with the revised absolute calibrations discussed in § III.

Individual *IUE* spectra are checked for anomalies before averaging. Spurious features due to reseaux, bright spots, and particle hits are removed by editing out appropriate wavelength intervals that are typically 20–30 Å wide. For a reseau, the flux is restored by a constant FN, which is the average of points on either side. Gross and background FN plots and image headers for each spectrum are also consulted to check overall data quality and identify processing irregularities. Cases in which the background or noise level is excessively high, or the flux level anomalously low, are rejected. For the five prime *IUE* standards, hundreds of spectra with optimum exposure times are available in the *IUE* data-bank (see Table 1), and the checking of individual spectra is automated (see Papers II and III). Radiation induced spots and blemishes are rare on images of stars with fluxes in the first 5 decades of the 6-decade dynamic range due to the relatively short exposure times.

In general, three or more spectra are required in each *IUE* camera range for a star to qualify as an *HST* standard, although one good quality trailed spectrum is allowed in the case of the bright star ζ Peg. In the averaging procedure, large-aperture spectra and most trailed spectra are used to define absolute flux levels. The effective exposure times of small-aperture spectra are computed by normalizing to the mean of the large-aperture spectra in the interval 1600–1725 Å for SWP spectra and 2600–2775 Å for LW spectra. If these first choice regions contain saturated data, second choice regions of 1300–1500 Å and 2235–2360 Å are used. A few spectra from fast trails which are found to have marginally low overall flux levels are treated as small aperture spectra. Spectra derived from multiple exposures in the large apertures are treated as small-aperture spectra, due to the possibility that flux is lost at the ends of the large aperture when a target is positioned off-center along the major axis. In order to improve data quality in spectral regions where the *IUE* cameras have relatively low sensitivity, many spectra are included with broad regions of overexposure. The data points flagged as saturated are not included in the co-additions. Averaging is performed by accumulating the sums of calibrated net spectra, ΣA, for each wavelength point and summing the corresponding exposure times and effective exposure times, Σt. The absolute flux, in erg cm^{-2} s^{-1} $Å^{-1}$, is derived by computing $\Sigma A/\Sigma t$ at each point. The spectra are all resampled at the mean sampling interval of *IUE* production processing, 1.1797 Å and 1.8693 Å for SWP and LW, respectively, before co-adding. The resampling reduces the noise and introduces more correlation between neighboring samples but does not significantly reduce the resolution of 5–6 Å.

At each wavelength, an RMS scatter σ is also computed. This σ is an RMS scatter of the flux measurements of the co-added spectra using the individual exposure times as weights. To account for the cases in which only one spectrum contributes, or where σ is too low due to statistical fluctuations, all σ values less than 3% are set to 3%. The few points with negative flux or with σ greater than 150% are eliminated. The short wavelength cutoff of all SWP spectra is 1148 Å, while the long wavelength cutoff of the LW spectra is the first point beyond 3170 Å where σ is greater than 19.5% or where there is only one spectrum in the co-addition. In the wavelength region of overlap between cameras, the switch from SWP to

LW fluxes is usually at 1970 Å. However, SWP fluxes are used at longer wavelengths in the composite fluxes of the three cool stars because of the high noise level in the LW fluxes of these stars. The criteria in these cases is to use the SWP flux where the LW flux is negative or the LW σ exceeds 20%, out to the last SWP point at about 1989 Å.

The co-addition of the LW fluxes for the hundreds of optimum exposures of the five *IUE* standard stars is a special case. The LWP and LWR spectra for each star are averaged separately and trimmed at the long wavelength end, as described above. The average LWP and LWR spectra are combined into one final LW spectrum by weighting each point by $1/\sigma_\mu^2$, where the estimated error in the mean, σ_μ, is σ divided by the fourth root of the number of spectra, N, in each co-addition. The expected reduction in σ would be $\sqrt{N}$ for normal statistics, but the fixed pattern noise in *IUE* spectra causes the point-to-point scatter to drop more slowly than expected for co-added spectra.

The resulting average spectra are plotted in Figures 3 and 4. The digital spectra are in the STScI Calibration Data Base System and will be available to the astronomical community via the STScI Data Management Facility. The region of Lyα from 1200–1226 Å is not plotted but is retained in the digital versions of the spectra. For the fainter stars, the Lyα region is contaminated by the geocoronal emission line. No attempt to correct for this contaminant is made. For the brightest stars, Lyα is uncontaminated, but the flux at the line center is so low that our logarithmic plots are confused by attempting to illustrate this region of the spectrum.

The spectra of the three cool stars in Figure 4 are contaminated by long-wavelength light that is scattered from the grating. This contaminant is evidenced by the upturn in apparent flux in the 1200 Å region. In fact, the continuum below about 1600 Å may be dominated by this artifact. Basri, Clarke, and Haisch (1985) have proposed a correction algorithm for scattered light (see also Harris and Sonneborn 1987, and references therein). However, the uncorrected *IUE* fluxes are presented in anticipation of a better solution from the requirement that *IUE*, FOS, and GHRS flux determinations must agree for these cool stars.

The numbers listed in columns 14 and 15 of Table 1, headed σ_{SWP} and σ_{LW}, are the RMS scatter averaged over the points in the wavelength ranges 1280–1970 Å and 1970–3200 Å, respectively. The values of σ_{SWP} and σ_{LW} are relatively high for the cool stars β Hyi, HD 27836, and 16 Cyg B and, to a lesser extent, for the faintest white dwarfs HZ 4, LB 227, and LDS 749B. In the case of the cool stars, large values of σ are caused by the steep drop in flux towards shorter wavelengths. For these cool stars, the *IUE* cameras have insufficient dynamic range to give good signal-to-noise over the whole spectrum. In the case of the faintest white dwarfs, long exposure times preclude the use of the observational techniques described in §II to improve the signal-to-noise ratio. Furthermore, the radiation-induced background level in the *IUE* cameras increases with exposure duration. Consequently, the signal-to-noise ratios for these stars are lower than for the brighter stars. Some stars, such as γ UMa and ξ^2 Cet, have relatively low values of σ_{SWP} and/or σ_{LW}. In these cases, the average flux distributions are based predominantly on small numbers of high quality spectra taken in the same observing runs. Noise patterns in these spectra due to the time-dependent 'fixed-pattern noise' (Welty 1988) are similar and result in relatively small RMS variations among the individual spectra.

Among the remaining stars, there are *no* abnormally large values of σ that might indicate intrinsic stellar variability or inconsistent flux measurements that could be attributed to *IUE* pointing errors.

V. COMPARISON WITH ALTERNATIVE ABSOLUTE FLUXES

The best estimates of the internal and external errors in the *IUE* fluxes are derived from comparisons with other measurements and with the predictions of models. The internal error (or relative error) is the error in the flux of one star relative to that of another star, while the external error (or absolute error) is the systematic error in the measured flux compared to the true flux of a star. To avoid confusion by random noise, the discussion is for errors in broad bands of the order of 100 Å in width.

a) OAO 2 and TD-1

The *OAO 2* fluxes of Code and Meade (1979) and the *TD-1* data from Jamar *et al.* (1976) are the most appropriate UV spectrophotometry to compare with our *IUE* fluxes. In Figures 5 a–f, the *IUE* fluxes for the six *OAO 2* reference standards are compared to the *TD-1* fluxes (open squares) and *OAO 2* fluxes (heavy solid line). The *OAO 2* and *TD-1* fluxes are corrected to the common *IUE* scale (Bohlin and Holm 1984). Except for a few isolated points, the *TD-1* and *IUE* fluxes are consistent over the 1360–2540 Å *TD-1* range to the accuracy of $\sim$ 2% that is discernable on the plots. Some systematic differences between the *OAO 2* and *IUE* fluxes exist, especially longward of the limit of the *TD-1* coverage. Temperature changes may affect the sensitivity of one or both of the *IUE* or *OAO 2* photocathodes at the longer wavelengths, where the energy of the photoelectrons is the smallest. The *OAO 2* flux of μ Col falls systematically below *IUE* by about 6% in the LW range. Consequently, the *IUE* calibration for LWR would produce fluxes about 1% higher, if μ Col had been omitted as a reference star. This 1% uncertainty is a crude estimate of the broadband error in the transfer of the reference flux scale from *OAO 2* to *IUE*.

In Figures 5g–l, *IUE* fluxes are compared with an independent set of *OAO 2* and *TD-1* spectra that are *not* used in deriving the *IUE* absolute calibrations for SWP and LWR. In general, agreement among the three sources of UV spectrophotometry is within a few percent; and no evidence is seen for errors that are systematic for all stars. One problem in the *IUE* spectra of α Leo and α Lyr is a noisy bump of 5–10% in the 2000–2100 Å region. The *IUE* flux for these two stars is defined mostly by LWP spectra processed with ITF2. Below 2300 Å, ITF2 introduces more positive noise spikes than ITF1, especially for overexposures, where the ITF is often extrapolated. Many of the α Leo and α Lyr spectra are overexposed to bring up the signal where LWP is relatively insensitive. In order to achieve the moderate data quality shown in Figures 5i and k, many noise clumps have been removed from the individual LWP spectra at the shorter wavelengths.

Shown in Figures 5m–p are the comparisons for γ UMa and ζ Oph and for the faint *TD-1* stars BD+75°325 and BD+28°4211. Noise in the *TD-1* spectra limits the precision of the comparison, especially at the longer wavelengths. Not shown is the faintest *TD-1* star BD+33°2642, where noise dominates the *TD-1* data. For ζ Oph, the *IUE* flux is below the *OAO 2* and *TD-1* measurements by 5–10% at all wavelengths. Taylor (1984) discusses the variability of ζ Oph for ground-based observations. However, ζ Oph is included for studies of scattered light in the centers of the strong interstellar lines and is not a spectrophotometric standard.

b) ANS

The best check on *IUE* spectrophotometry in broad bands is provided by the UV photometry from the *ANS* satellite (Wesselius *et al.* 1982), which has a repeatability of about 1% for all but the faintest of our stars. Figure 6 compares *ANS* photometry to the mean *IUE* fluxes averaged over the *ANS* bandpasses. The one sigma scatter of the points about the mean are 2.8% (1550 Å), 2.1% (1800 Å), 1.2% (2200 Å), and 2.0% (2500 Å). This rms scatter of 1–3% in the ratios of *IUE* to *ANS* over a dynamic range of more than 10^4 in flux is indicative of an expected photometric repeatability for *IUE* of about 2%, after correcting for the small *ANS* contribution to the scatter. *ANS* measurements with an uncertainty greater than 3% are not used. Because of the sparsity of data, systematic effects of a few percent cannot be ruled out, especially in the lower two decades of flux in Figure 6.

The four dashed lines in Figure 6 are drawn at the mean values of the ratios of *IUE* flux to *ANS* published flux. The mean values are 1.084, 1.003, 0.939, and 1.011 at 1500, 1800, 2200, and 2500 Å, respectively, which compare favorably to the previously published *ANS* corrections of 1.083, 0.995, 0.909, and 1.046 (Bohlin, Harrington, and Stecher 1982; Bohlin and Holm 1984). The difference between these values of $< 1\%$ for SWP and $< 4\%$ for LW are measures of the amount of residual error that might still be present in transfer of the common flux scale to *IUE*.

c) Ground-Based

The agreement between the *IUE* and the ground-based fluxes for the primary optical standard α Lyr is shown in Figure 7 at wavelengths below the Balmer discontinuity. In order to compare *IUE* with the ground-based data, a 10,300° K Planck function is shown normalized to the *IUE* data in the 3200–3300 Å range. The ratio and one sigma scatter of the ground-based measurements to the Planck function is 1.014 ± 0.008 for the 5 points of Oke and Gunn (1983) and $1.014 \pm .013$ for the 6 points of Hayes and Latham (1975). Similarly, the ratios of the Stone (1977) data between 3300 and 3600 Å to *IUE* range from 1.001 ± 0.010 to 1.034 ± 0.010 for Feige 34, BD+33°2642, BD+28°4211, and Feige 110. The Stone fluxes represent a transfer of the measurements of Hayes and Latham for the primary standard α Lyr to the fainter secondary standards.

d) Model Atmospheres

The comparison of measured fluxes with model atmosphere calculations provides a good check on the *IUE* calibration, which is based ultimately on the physics of laboratory standards. A model for a pure hydrogen white dwarf is a particularly good comparison, because the lack of heavy elements simplifies the computation of line blanketing and because the proximity of the brighter white dwarfs minimizes any extinction by the dust. Figure 8 shows the ratio of the G191B2B *IUE* flux to a model with $T_e = 62,250$ K and $\log g = 7.55$ provided by Holberg (1988). The temperature and gravity are determined by fitting the model to the broad stellar Lyα line. Longward of 1300 Å, *IUE*/model flux ratios that agree to 5% with Figure 8 are found for several other white dwarfs (Holberg 1988, Finley 1988). Furthermore, the results of Hackney, Hackney, and Kondo (1982) are consistent to 5% for the ratio of the re-calibrated *IUE* fluxes to their model fluxes for BL Lac objects in the SWP camera range. The structure in the flux ratio of Figure 8 may be caused by errors in the flux distribution originally chosen for the fundamental UV standard η UMa. However, the mean offset from unity of the IUE/model flux ratio for G191B2B could be caused by an extinction by the dust of only E(B-V) = 0.01.

In summary, the model predictions suggest that the *IUE* fluxes may be low by $\sim$ 10%. The magnitude of this difference between the model and *IUE* is consistent with the uncertainty of the η UMa fluxes of Bohlin *et al.* (1980). To resolve this discrepancy, more work is needed in rocket-UV flux measurements and in comparing model atmosphere calculations to the data over a broad range of physical conditions.

VI. SUMMARY

Absolute *IUE* flux distributions are presented for 37 *HST* calibration stars ranging in brightness from η UMa ($V = 1.86$) to LDS 749B ($V = 15.35$). These results are the product of a long-term collaborative program of the Space Telescope Science Institute and the VILSPA *IUE* Observatory. In order to maximize the accuracy of the fluxes, re-calibrations of the *IUE* SWP and LWR cameras have been derived using point source observations and high-speed trailed spectra of the six bright *OAO 2* standard stars obtained in 1984–5 by the *IUE* project. For the reprocessing of the entire *IUE* data archive, the current plan is to base the new absolute calibrations on the same data-set. Thus, *HST* fluxes calibrated with the absolute fluxes presented in this work should be compatible with the reprocessed *IUE* archive. The final flux distributions include corrections for the change in camera sensitivity with time and the different relative sensitivities of the large aperture, small aperture, and trailed observing modes. In general, the re-calibration reduces SWP and LWR fluxes by as much as 10%.

In general, the *IUE* fluxes agree with the *OAO 2*, *TD-1*, and *ANS* data to a few percent for stars in common, confirming the accuracy of the transfer of the η UMa reference flux scale and the 2% RMS internal consistency of the *IUE* spectrophotometry in bands of $\geq$ 100 Å over a dynamic range of 10^4. Comparisons with white dwarf model atmospheres indicate the absolute accuracy of the *IUE* fluxes is within 10–15%, while a comparison with ground-based data demonstrates an accuracy of $\sim$ 3% for the *IUE* absolute fluxes at the longest wavelengths.

Acknowledgements

Drs. C. C. Wu and J. C. Blades were Principal Investigators on the first NASA and ESA observing proposals for this program, respectively. We wish to thank the staff at both *IUE* groundstations and Drs. C. Grady and O. Lupie for their assistance with the observations. Dr. N. Oliversen provided calibration data and results prior to publication. We are grateful to Drs. Y. Kondo and W. Wamsteker for their support of this program. AWH thanks the Space Telescope Science Institute for its hospitality and travel support under the Visitor Program during the completion of this work. The efforts of D. Lindler were essential to the recalibration and the production of the Figures.

REFERENCES

Basri, G., Clarke, J. T., and Haisch, B. M. 1985, *Astr. Ap.*, **144**, 161.

Boggess, A., *et al.* 1978, *Nature*, **275**, 377.

Bohlin, R. C. 1986, *Ap. J.*, **308**, 1001 (Paper I).

Bohlin, R. C. 1988, in *New Directions in Spectrophotometry*, eds. A. G. Davis Philip, D. S. Hayes, and S. J. Adelman (Schenectady, NY: L. Davis), p. 121.

Bohlin, R. C., Blades, J. C., Holm, A. V., Savage, B. D., and Turnshek, D. A. 1987, *Standard Astronomical Sources for HST: 1. UV Spectrophotometric Standards* (ST ScI).

Bohlin, R. C., and Grillmair, C. J. 1988a, *Ap. J. Suppl.*, **66**, 209 (Paper II).

Bohlin, R. C., and Grillmair, C. J. 1988b, *Ap. J. Suppl.*, **68**, 487 (Paper III).

Bohlin, R. C., Harrington, J. P., and Stecher, T. P. 1982, *Ap. J.*, **252**, 635.

Bohlin, R. C., and Holm, A. V. 1980, *NASA IUE Newsletter*, **10**, 37 (= 1981, *ESA IUE Newsletter*, **11**, 18).

Bohlin, R. C., and Holm A. V. 1984, *NASA IUE Newsletter*, **24**, 74 (= 1984, *ESA IUE Newsletter*, **20**, 22).

Bohlin, R. C., Holm, A. V., Savage, B. D., Snijders, M. A. J., and Sparks, W. M. 1980, *Astr. Ap.*, **85**, 1.

Cassatella, A., and Harris, A. W. 1983, *ESA IUE Newsletter*, **17**, 12 (= 1983, *NASA IUE Newsletter*, **23**, 21).

Cassatella, A., Lloyd, C., and Riestra, R. G. 1988, *ESA IUE Newsletter*, **31**, 13 (= 1988, *NASA IUE Newsletter*, **35**, 225).

Code, A. D., and Meade, M. R. 1979, *Ap. J. Suppl.*, **39**, 195.

Finley, D. 1988, private communication.

FitzGerald, M. P. 1970, *Astr. Ap.*, **4**, 234.

Hackney, R. L., Hackney, K. R. H., and Kondo, Y. 1982, in *Advances in UV Astronomy: Four Years of IUE Research*, Y. Kondo, J. M. Meade, and R. D. Chapman, eds., (NASA CP-2238), p. 335.

Harris, A. W., and Cassatella, A. 1985, *ESA IUE Newsletter*, **22**, 9.

Harris, A. W., and Sonneborn, G. 1987, in *Exploring the Universe with the IUE Satellite*, eds. Y. Kondo, *et al.* (Dordrecht: D. Reidel), p. 729.

Hayes, D. S., and Latham, D. W. 1975, *Ap. J.*, **197**, 593.

Hoffleit, D. 1964, *Catalogue of Bright Stars*, (Yale University Observatory).

Holberg, J. 1988, private communication.

Holm, A. V., Bohlin, R. C., Cassatella, A., Ponz, D. P., and Schiffer, F. H. 1982, *Astr. Ap.*, **112**, 341.

Imhoff, C. L. 1989, *NASA IUE Newsletter*, **37**, 122.

Jamar, C., Macau-Hercot, D., Monfils, A., Thompson, G. I., Houziaux, L., and Wilson, R. 1976, *UV Bright-Star Spectrophotometric Catalogue*, ESA SR-27.

Johnson, H. L., Mitchell, R. I., Iriarte, B., and Wiśniewski, W. Z. 1966, *Comm. Lunar Plan. Obs.*, **4**, 99.

Lindler, D. J., and Bohlin, R. C. 1986, CAL/FOS-032 (ST ScI).

McCook, G. P., and Sion, E. M. 1984, *A Catalogue of Spectroscopically Identified White Dwarfs, 2nd Ed.* (Villanova, Pa.: Villanova Press).

Nicolet, B. 1978, *Astr. Ap. Suppl.*, **34**, 1.

Oke, J. B., and Gunn, J. E. 1983 *Ap. J.*, **266**, 713.

Oliversen, N. A. 1986, *NASA IUE Newsletter*, **31**, 40.
Oliversen, N. A. 1988, *NASA IUE Newsletter*, **35**, 55.
Panek, R. J. 1982, *NASA IUE Newsletter*, **18**, 68.
Stone, R. P. S. 1977, *Ap. J.*, **218**, 767.
Taylor, B. 1984, *Ap. J. Suppl.*, **54**, 259.
Turnshek, D. A., Baum, W. A., Bohlin, R. C., Dolan, J. F., Horne, K., Koorneef, J., Oke, J. B., Williamson II, R. L. 1989, *Standard Astronomical Sources for HST: 2. Optical Calibration Targets* (ST ScI).
Welty, D. 1988, *NASA IUE Newsletter*, **34**, 24.
Wesselius, P. R., van Duinen, R. J., de Jonge, A. R. W., Aalders, J. W. G., Luinge, W., and Wildeman, K. J. 1982, *Astr. Ap. Suppl.*, **49**, 427.

TABLE 1
UV STANDARD STARS FOR HST

1 HD	2 Name	3 $\alpha(2000)^b$	4 $\delta\ (2000)^b$	5 Sp.T.	6 V	7 $B-V$	8 $E(B\text{-}V)$	9 Ecl. Lat.	10 SWP[c]	11 LWR[c]	12 LWP[c]	13 $Tot.^c$	14 σ_{SWP}	15 σ_{LW}
2151	β Hyi	S 0^h 25^m 45.38^s	−77° 15′ 15.″5	G2IV	2.80	+0.62	−0.02	−65°	5, 0, 1	0, 3, 1	···	10	0.089	0.123
3360	ζ Cas	S 0 36 58.30	+53 53 48.9	B2IV	3.66	−0.20	0.04	+45	12, 11, 5	8, 4, 6	···	46	0.044	0.059
···	BPM 16274	0 50 03.18	−52 08 17.4	DA2	14.20	−0.02	···	−51	7, 0, 0	···	6, 0, 0	13	0.041	0.068
15318	ξ^2 Cet	S 2 28 09.53	+8 27 36.3	B9III	4.28	−0.06	0.02	−6	0, 3, 0	···	1, 2, 0	6	0.016	0.013
···	GD50	3 48 50.06	−0 58 30.4	DA2	14.05	−0.28	···	−20	3, 0, 3	···	2, 0, 1	9	0.046	0.054
···	HZ 4	3 55 21.70	+9 47 18.7	DA4	14.47	+0.08	···	−10	3, 0, 0	···	4, 0, 0	7	0.050	0.102
···	LB227	4 09 28.76	+17 07 54.4	DA4	15.35	+0.05	···	−4	5, 0, 0	···	7, 0, 0	12	0.067	0.126
···	HZ 2	4 12 43.51	+11 51 50.4	DA3	13.86	−0.05	···	−9	5, 0, 0	···	6, 0, 0	11	0.041	0.078
27836	···	4 24 12.33	+14 45 30.7	G1V	7.62	+0.60	−0.02	−7	2, 0, 0	2, 1, 1	···	6	0.356	0.223
···	G191-B2B	5 05 30.62	+52 49 54.0	DA0	11.78	−0.34	···	+30	6, 12, 3	1, 0, 0	5, 0, 2	29	0.046	0.068
32630	η Aur	S 5 06 30.86	+41 13 34.0	B3V	3.18	−0.18	0.02	+18	8, 2, 3	8, 4, 4	···	29	0.041	0.058
34816	λ Lep	S 5 19 34.49	−13 10 36.5	B0.5V	4.28	−0.27	0.01	−36	11, 3, 3	7, 6, 4	···	34	0.046	0.054
38666	μ Col	S 5 45 59.92	−32 18 23.4	O9V	5.17	−0.28	0.03	−56	11, 7, 5	8, 6, 4	···	41	0.039	0.053
49798	···	6 48 04.64	−44 18 59.3	O6	8.27	−0.30	0.02	+67	5, 3, 2	0, 2, 0	4, 1, 1	18	0.034	0.068
60753[a]	···	S 7 33 27.26	−50 35 03.7	B3IV	6.70	−0.09	0.11	−70	135, 78, 69	65, 52, 45	57, 55, 19	575	0.041	···
···	BD+75°325[a]	8 10 49.31	+74 57 57.5	O5p	9.55	−0.36	−0.04	+53	149, 42, 67	70, 20, 52	78, 19, 24	521	0.048	···
···	AGK+81°266	9 21 19.06	+81 43 28.6	sdO	11.85	−0.34	···	+61	11, 1, 1	1, 0, 1	9, 0, 1	25	0.045	0.075
···	GD108	10 00 47.33	−7 33 31.2	sdB?	13.56	−0.23	···	−18	2, 0, 1	···	2, 0, 1	6	0.030	0.048
87901	α Leo	S10 08 22.32	+11 58 02.0	B7V	1.35	−0.11	0.02	+0.5	5, 10, 1	0, 1, 1	3, 8, 1	30	0.050	0.042
···	Feige 34	10 39 36.71	+43 06 10.1	DO	11.12	−0.30	···	+32	3, 2, 2	···	11, 4, 4	26	0.032	0.054
93521[a]	···	10 48 23.51	+37 34 12.8	O9Vp	7.04	−0.28	0.03	+27	103, 23, 62	64, 8, 46	47, 15, 12	380	0.054	···
103287	γ UMa	S11 53 49.83	+53 41 41.1	A0V	2.44	0.00	0.01	+47	0, 2, 0	1, 1, 1	···	5	0.011	0.060
···	HZ 21	12 13 56.42	+32 56 30.8	DO2	14.68	−0.36	···	+31	10, 0, 3	2, 0, 1	9, 0, 0	25	0.048	0.084
···	HZ 44	13 23 35.37	+36 08 00.0	sdO	11.71	−0.27	···	+41	4, 3, 0	0, 1, 0	3, 1, 0	12	0.037	0.050
···	GRW+70°5824	13 38 51.77	+70 17 08.5	DA3	12.79	−0.09	···	+67	9, 0, 0	1, 0, 0	8, 0, 0	18	0.039	0.065
120315	η UMa	S13 47 32.44	+49 18 48.0	B3V	1.86	−0.19	0.01	+54	0, 9, 1	0, 13, 1	···	24	0.033	0.046
···	BD+33°2642[a]	15 51 59.86	+32 56 54.8	B2IV	10.84	−0.17	0.07	+51	88, 0, 20	55, 0, 18	44, 0, 0	225	0.054	···
149757	ζ Oph	S16 37 09.54	−10 34 01.7	O9.5V	2.56	+0.02	0.32	+11	0, 3, 0	0, 1, 0	0, 1, 0	5	0.033	0.025
172167	α Lyr	S18 36 56.33	+38 47 01.1	A0V	0.03	0.00	0.01	+62	3, 6, 0	···	4, 9, 0	22	0.054	0.041
186427	16 CygB	S19 41 51.96	+50 31 02.9	G5V	6.20	+0.66	−0.02	+69	2, 0, 1	1, 4, 25	9, 0, 3	45	0.576	0.402
···	LDS 749B	21 32 15.75	+0 15 13.6	DB4	14.73	−0.04	···	+14	3,0, 0	2, 0, 0	2, 0, 0	7	0.065	0.107
···	BD+28°4211[a]	21 51 11.07	+28 51 51.8	Op	10.53	−0.34	−0.02	+39	134, 38, 36	72, 13, 45	69, 16, 24	447	0.047	···
···	G93-48	21 52 25.33	+2 23 24.3	DA3	12.74	−0.01	···	+14	2, 0, 1	···	2, 0, 1	6	0.034	0.052
···	NGC7293	22 29 38.46	−20 50 13.3	V.Hot	13.43	−0.34	0.01	−11	9, 1, 1	5, 0, 0	5, 0, 0	21	0.048	0.073
214680	10 Lac	S22 39 15.70	+39 03 01.1	O9V	4.88	−0.20	0.11	+43	15, 5, 2	8, 5, 3	···	38	0.041	0.055
214923	ζ Peg	S22 41 27.74	+10 49 52.9	B8V	3.40	−0.09	0.02	+18	0, 1, 0	···	0, 1, 0	2	···	···
···	Feige 110	23 19 58.39	−5 09 55.8	D0p	11.50	−0.30	···	−1	7, 0, 1	1, 0, 0	4, 0, 4	17	0.040	0.068

[a]IUE prime standard

[b]Coordinates preceded by S are from the SAO catalog and include corrections for proper motion to epoch 2000. Other coordinates are from the ST ScI Guide Star Selection System and have not been corrected for proper motion. The plates are epoch 1975–1985. For proper motion data and further details see Bohlin *et al.* (1987) and Turnshek *et al.* (1989).

[c]Numbers of IUE spectra used in generating the mean plots in Figs. 3, 4 listed by observing mode: large aperture, trailed, sum of small aperture plus multiple exposures in the large aperture.

TABLE 2
S/L AND T/L RELATIVE SENSITIVITIES

λ (Å)	S/L[a]	T/L[b]	λ (Å)	S/L[a]	T/L[b]	S/L[a]	T/L[b]	S/L[a]	T/L[b]
	SWP			LWP (ITF1)		LWP (ITF2)		LWR	
1150	0.970	1.069	1850	1.000	1.075	1.090	1.100	1.113	1.058
1175	0.977	1.050	1900	1.000	1.072	1.072	1.100	1.063	1.056
1200	0.983	1.034	1950	0.998	1.069	1.052	1.100	1.024	1.053
1225	0.989	1.019	2000	0.983	1.066	1.032	1.100	0.998	1.051
1250	0.995	1.005	2050	0.955	1.064	1.012	1.100	0.981	1.049
1275	0.999	0.997	2100	0.945	1.062	0.992	1.100	0.973	1.047
1300	1.002	0.991	2150	0.950	1.060	0.974	1.100	0.971	1.045
1325	1.005	0.990	2200	0.969	1.059	0.975	1.100	0.971	1.043
1350	1.008	0.991	2250	0.996	1.058	1.005	1.094	0.971	1.041
1375	1.011	0.996	2300	1.014	1.057	1.039	1.084	0.973	1.039
1400	1.014	1.002	2350	1.023	1.056	1.042	1.073	0.986	1.038
1425	1.016	1.007	2400	1.028	1.055	1.035	1.062	1.002	1.039
1450	1.017	1.012	2450	1.030	1.054	1.027	1.056	1.021	1.040
1475	1.018	1.018	2500	1.029	1.053	1.019	1.052	1.032	1.040
1500	1.019	1.027	2550	1.025	1.052	1.011	1.048	1.040	1.040
1525	1.018	1.036	2600	1.018	1.051	1.003	1.045	1.047	1.041
1550	1.018	1.048	2650	1.007	1.051	0.997	1.044	1.050	1.041
1575	1.017	1.051	2700	0.997	1.052	0.992	1.045	1.052	1.041
1600	1.016	1.052	2750	0.993	1.053	0.988	1.046	1.048	1.042
1625	1.015	1.053	2800	0.995	1.055	0.985	1.048	1.042	1.042
1650	1.013	1.052	2850	0.998	1.058	0.984	1.050	1.036	1.043
1675	1.011	1.049	2900	1.000	1.061	0.983	1.052	1.030	1.043
1700	1.008	1.042	2950	1.000	1.066	0.981	1.057	1.022	1.044
1725	1.005	1.035	3000	1.000	1.071	0.979	1.065	1.014	1.046
1750	1.002	1.030	3050	1.000	1.076	0.977	1.075	1.000	1.053
1775	0.999	1.028	3100	1.000	1.081	0.975	1.091	0.956	1.063
1800	0.995	1.027	3150	1.000	1.085	0.973	1.108	0.825	1.068
1825	0.990	1.028	3200	1.000	1.089	0.971	1.116	0.735	1.070
1850	0.984	1.028	3250	1.000	1.093	0.967	1.123	0.686	1.070
1875	0.978	1.027	3300	1.000	1.097	0.963	1.128	0.642	1.070
1900	0.972	1.026	3350	1.000	1.101	0.960	1.130	0.614	1.070
1925	0.966	1.024							
1950	0.960	1.022							
1975	0.954	1.020							

[a]Ratio of small-aperture (S) response to the large-aperture (L) response for point sources. Since the *IUE* small aperture is not a photometric aperture, the average of S/L over all wavelengths is normalized to unity. The relative small and absolute large aperture inverse sensitivities are related by

$$S^{-1}(\mathrm{S}) = S^{-1}(\mathrm{L})/(\mathrm{S/L}).$$

[b]Ratio of trailed (T) response to point sources in the large aperture. The absolute calibrations are related by

$$S^{-1}(\mathrm{T}) = S^{-1}(\mathrm{L})/(\mathrm{T/L}).$$

The values of T/L are for trailed exposure times computed using lengths for the large apertures of 21.″4 for SWP and 20.″5 for LW spectra (Panek 1982).

TABLE 3A
ABSOLUTE CALIBRATION FOR SWP ITF2

λ (Å)	S^{-1}[a]	λ (Å)	S^{-1}	λ (Å)	S^{-1}	λ (Å)	S^{-1}	λ (Å)	S^{-1}
1150	19.610	1325	2.036	1500	3.283	1675	2.830	1850	1.874
1155	15.220	1330	2.041	1505	3.328	1680	2.790	1855	1.872
1160	12.390	1335	2.048	1510	3.371	1685	2.750	1860	1.871
1165	10.410	1340	2.057	1515	3.409	1690	2.709	1865	1.870
1170	8.913	1345	2.068	1520	3.442	1695	2.667	1870	1.869
1175	7.741	1350	2.081	1525	3.469	1700	2.625	1875	1.869
1180	6.789	1355	2.096	1530	3.491	1705	2.582	1880	1.869
1185	5.997	1360	2.113	1535	3.507	1710	2.538	1885	1.869
1190	5.326	1365	2.132	1540	3.517	1715	2.495	1890	1.868
1195	4.751	1370	2.153	1545	3.523	1720	2.452	1895	1.868
1200	4.264	1375	2.176	1550	3.523	1725	2.409	1900	1.867
1205	3.855	1380	2.201	1555	3.519	1730	2.368	1905	1.867
1210	3.512	1385	2.227	1560	3.510	1735	2.327	1910	1.866
1215	3.226	1390	2.256	1565	3.498	1740	2.288	1915	1.865
1220	2.987	1395	2.287	1570	3.482	1745	2.251	1920	1.863
1225	2.789	1400	2.319	1575	3.463	1750	2.214	1925	1.862
1230	2.625	1405	2.354	1580	3.441	1755	2.180	1930	1.861
1235	2.491	1410	2.391	1585	3.416	1760	2.147	1935	1.859
1240	2.383	1415	2.429	1590	3.390	1765	2.116	1940	1.858
1245	2.299	1420	2.470	1595	3.362	1770	2.087	1945	1.856
1250	2.233	1425	2.512	1600	3.333	1775	2.059	1950	1.854
1255	2.181	1430	2.556	1605	3.304	1780	2.034	1955	1.852
1260	2.141	1435	2.603	1610	3.273	1785	2.011	1960	1.850
1265	2.111	1440	2.650	1615	3.243	1790	1.989	1965	1.848
1270	2.088	1445	2.700	1620	3.212	1795	1.970	1970	1.846
1275	2.071	1450	2.751	1625	3.180	1800	1.953	1975	1.844
1280	2.059	1455	2.804	1630	3.148	1805	1.938	1980	1.842
1285	2.050	1460	2.857	1635	3.116	1810	1.925	1985	1.841
1290	2.044	1465	2.911	1640	3.083	1815	1.914	1990	1.839
1295	2.039	1470	2.966	1645	3.049	1820	1.905	1995	1.837
1300	2.035	1475	3.021	1650	3.015	1825	1.897	2000	1.835
1305	2.032	1480	3.076	1655	2.979	1830	1.890		
1310	2.031	1485	3.130	1660	2.943	1835	1.885		
1315	2.031	1490	3.183	1665	2.906	1840	1.880		
1320	2.033	1495	3.234	1670	2.869	1845	1.877		

[a] *IUE* inverse sensitivities for a point source centered in the large aperture. The stellar flux $F(\lambda)$ in erg cm^{-2} s^{-1} Å^{-1} is

$$F(\lambda) = S^{-1}(\lambda)\frac{\mathrm{FN}(\lambda)}{t},$$

where FN(λ) is the linearized *IUE* response in Flux Numbers and t is the exposure time in seconds.

TABLE 3B
ABSOLUTE CALIBRATION FOR LWR ITF1

λ (Å)	S^{-1}[a]	λ (Å)	S^{-1}	λ (Å)	S^{-1}	λ (Å)	S^{-1}	λ (Å)	S^{-1}
1850	15.150	2175	1.425	2500	0.507	2825	0.326	3150	1.244
1855	13.250	2180	1.415	2505	0.500	2830	0.327	3155	1.300
1860	11.730	2185	1.404	2510	0.492	2835	0.327	3160	1.360
1865	10.480	2190	1.392	2515	0.485	2840	0.328	3165	1.424
1870	9.394	2195	1.378	2520	0.477	2845	0.329	3170	1.492
1875	8.442	2200	1.364	2525	0.470	2850	0.330	3175	1.566
1880	7.596	2205	1.349	2530	0.464	2855	0.331	3180	1.645
1885	6.853	2210	1.333	2535	0.457	2860	0.332	3185	1.730
1890	6.207	2215	1.316	2540	0.450	2865	0.333	3190	1.822
1895	5.650	2220	1.299	2545	0.444	2870	0.335	3195	1.920
1900	5.170	2225	1.281	2550	0.438	2875	0.336	3200	2.025
1905	4.757	2230	1.263	2555	0.432	2880	0.338	3205	2.139
1910	4.402	2235	1.244	2560	0.426	2885	0.340	3210	2.261
1915	4.096	2240	1.225	2565	0.421	2890	0.342	3215	2.393
1920	3.830	2245	1.206	2570	0.415	2895	0.345	3220	2.534
1925	3.597	2250	1.187	2575	0.410	2900	0.347	3225	2.686
1930	3.392	2255	1.167	2580	0.405	2905	0.350	3230	2.848
1935	3.209	2260	1.147	2585	0.400	2910	0.354	3235	3.022
1940	3.046	2265	1.128	2590	0.396	2915	0.357	3240	3.207
1945	2.900	2270	1.108	2595	0.391	2920	0.361	3245	3.404
1950	2.768	2275	1.088	2600	0.387	2925	0.365	3250	3.613
1955	2.648	2280	1.069	2605	0.383	2930	0.370	3255	3.836
1960	2.539	2285	1.049	2610	0.379	2935	0.375	3260	4.073
1965	2.440	2290	1.030	2615	0.375	2940	0.380	3265	4.326
1970	2.350	2295	1.011	2620	0.372	2945	0.386	3270	4.596
1975	2.267	2300	0.992	2625	0.368	2950	0.392	3275	4.884
1980	2.191	2305	0.974	2630	0.365	2955	0.398	3280	5.192
1985	2.121	2310	0.955	2635	0.362	2960	0.405	3285	5.521
1990	2.057	2315	0.937	2640	0.359	2965	0.412	3290	5.875
1995	1.998	2320	0.920	2645	0.356	2970	0.420	3295	6.256
2000	1.943	2325	0.903	2650	0.353	2975	0.428	3300	6.669
2005	1.893	2330	0.886	2655	0.351	2980	0.437	3305	7.119
2010	1.848	2335	0.869	2660	0.348	2985	0.446	3310	7.611
2015	1.805	2340	0.853	2665	0.346	2990	0.456	3315	8.154
2020	1.767	2345	0.838	2670	0.344	2995	0.466	3320	8.759
2025	1.731	2350	0.823	2675	0.342	3000	0.477	3325	9.442
2030	1.699	2355	0.808	2680	0.340	3005	0.488	3330	10.220
2035	1.669	2360	0.793	2685	0.338	3010	0.500	3335	11.130
2040	1.642	2365	0.779	2690	0.336	3015	0.512	3340	12.190
2045	1.618	2370	0.766	2695	0.335	3020	0.525	3345	13.490
2050	1.596	2375	0.752	2700	0.334	3025	0.539	3350	15.090
2055	1.577	2380	0.739	2705	0.332	3030	0.553		
2060	1.560	2385	0.727	2710	0.331	3035	0.568		
2065	1.545	2390	0.715	2715	0.330	3040	0.583		
2070	1.532	2395	0.703	2720	0.329	3045	0.599		
2075	1.521	2400	0.692	2725	0.328	3050	0.616		
2080	1.512	2405	0.681	2730	0.327	3055	0.634		
2085	1.504	2410	0.670	2735	0.327	3060	0.653		
2090	1.498	2415	0.659	2740	0.326	3065	0.673		
2095	1.493	2420	0.649	2745	0.326	3070	0.693		
2100	1.488	2425	0.639	2750	0.325	3075	0.715		
2105	1.485	2430	0.629	2755	0.325	3080	0.738		
2110	1.481	2435	0.619	2760	0.324	3085	0.762		
2115	1.479	2440	0.610	2765	0.324	3090	0.788		
2120	1.476	2445	0.600	2770	0.324	3095	0.815		
2125	1.474	2450	0.591	2775	0.324	3100	0.843		
2130	1.472	2455	0.582	2780	0.324	3105	0.873		
2135	1.469	2460	0.573	2785	0.324	3110	0.905		
2140	1.466	2465	0.565	2790	0.324	3115	0.939		
2145	1.463	2470	0.556	2795	0.324	3120	0.975		
2150	1.459	2475	0.548	2800	0.325	3125	1.013		
2155	1.454	2480	0.539	2805	0.325	3130	1.053		
2160	1.449	2485	0.531	2810	0.325	3135	1.097		
2165	1.442	2490	0.523	2815	0.325	3140	1.143		
2170	1.434	2495	0.515	2820	0.326	3145	1.192		

FIGURE CAPTIONS

Fig. 1 - Mean ratio of average spectra of the five *IUE* standard stars, based on a total of 151 LWP large-aperture spectra processed with LWP ITF2, to corresponding averages, based on a total of 295 large-aperture spectra processed with LWP ITF1. The ITF1 spectra are calibrated according to Cassatella and Harris (1983), as updated by Oliversen (1988), while the ITF2 spectra are calibrated per Cassatella, Lloyd, and Riestra (1988). There is overall agreement between the ITF1 and ITF2 fluxes to 1% in broad bands.

Fig. 2 - Comparison of LWP ITF1 fluxes with LWR fluxes. The ratio is based on 479 LWP spectra and 625 LWR spectra of the 5 *IUE* standard stars. The mean of the five ratios of average spectra is plotted, as in Fig. 1. The LWP/LWR ratio is $\sim$ 0.98% in the range 2100–2400 Å and $\sim$ 1.02% in the range 2500–2900 Å.

Fig. 3 - Average absolute *IUE* flux distributions of the hot *HST* standard stars. The revised absolute calibrations discussed in §III and corrections for S/L, T/L, and the time-dependent sensitivity changes are applied to individual spectra before averaging. Digital versions of the spectra will be available to the astronomical community through the STScI Data Management Facility.

Fig. 4 - Average absolute *IUE* flux distributions of the cool *HST* standard stars. See Fig. 3 caption.

Fig. 5 - Comparisons of UV flux measurements from *IUE* (*light line*), *OAO 2* (*heavy line*), and *TD-1* (*squares*). The *OAO 2* and *TD-1* fluxes are corrected to the same common scale on which the *IUE* calibration is based. The plots a–f are the six *OAO 2* stars used to transfer the common UV flux scale to *IUE*.

Fig. 6 - Ratio of the mean *IUE* to *ANS* flux in the four *ANS* bands as a function of flux for the stars in Table 1 for which *ANS* data are available (Wesselius *et al.* 1982). The dashed horizontal lines indicate the mean ratio in each band. The one sigma scatter of the flux ratios about the mean is less than 3% in each of the four bands over the full five-decade range in brightness. The *ANS* error bars that are larger than 3% are indicated.

Fig. 7 - Comparison of the *IUE* flux for α Lyr with the ground-based data of Oke and Gunn (1983) (*asterisks*) and Hayes and Latham (1975) (*squares*). The *light solid line* is a Planck function for 10,300 K that is normalized to the *IUE* data between 3200 and 3300 Å.

Fig. 8 - Ratio of the *IUE* flux for the white dwarf G191B2B to the predicted flux from a model atmosphere provided by Holberg (1988).

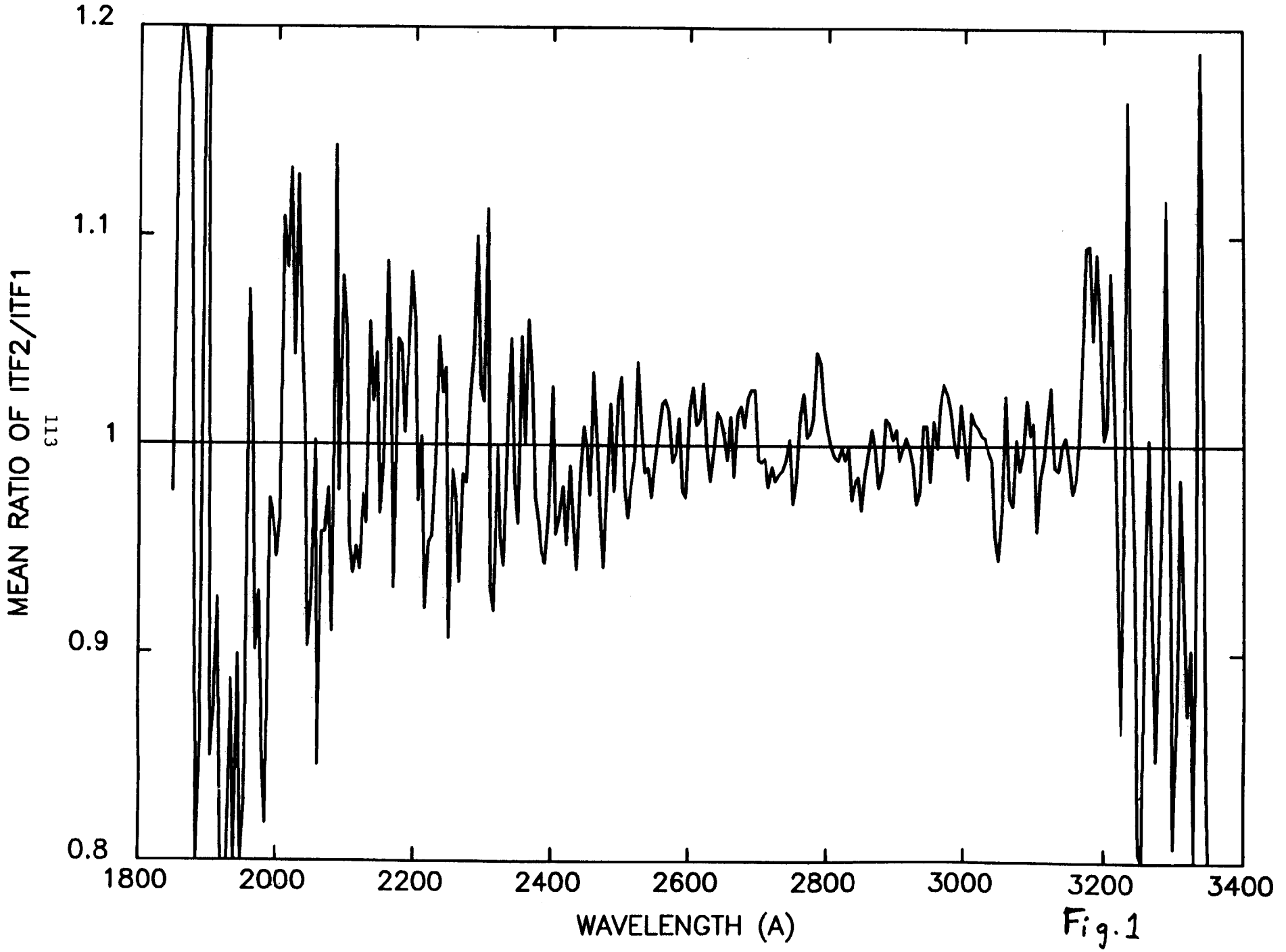
1.2
1.1
1
0.9
0.8
MEAN RATIO OF ITF2/ITF1
1800
2000
2200
2400
2600
2800
3000
3200
3400
WAVELENGTH (A)

Fig. 1

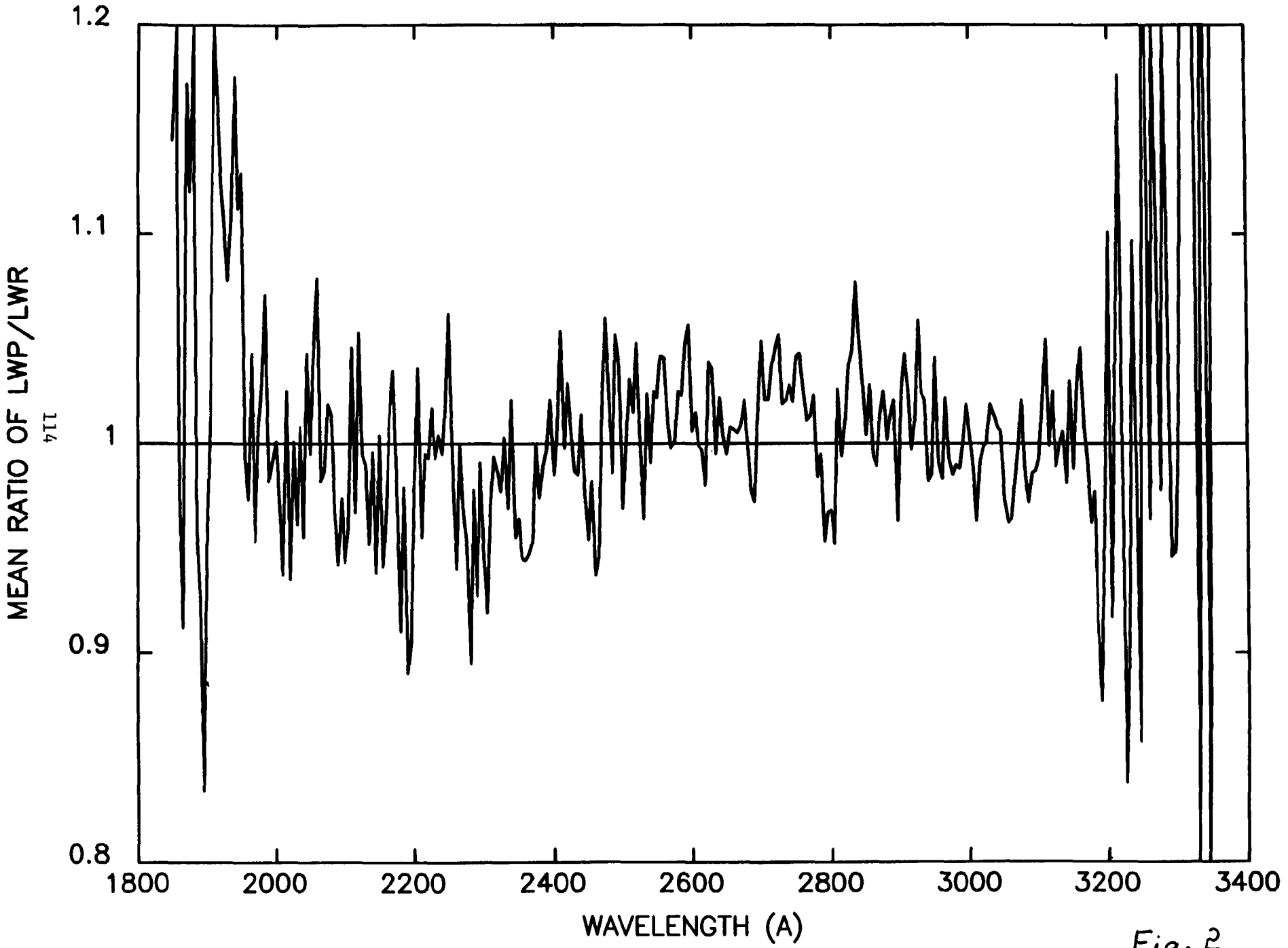
1.2
1.1
1
0.9
0.8
MEAN RATIO OF LWP/LWR
1800
2000
2200
2400
2600
2800
3000
3200
3400
WAVELENGTH (A)

Fig. 2

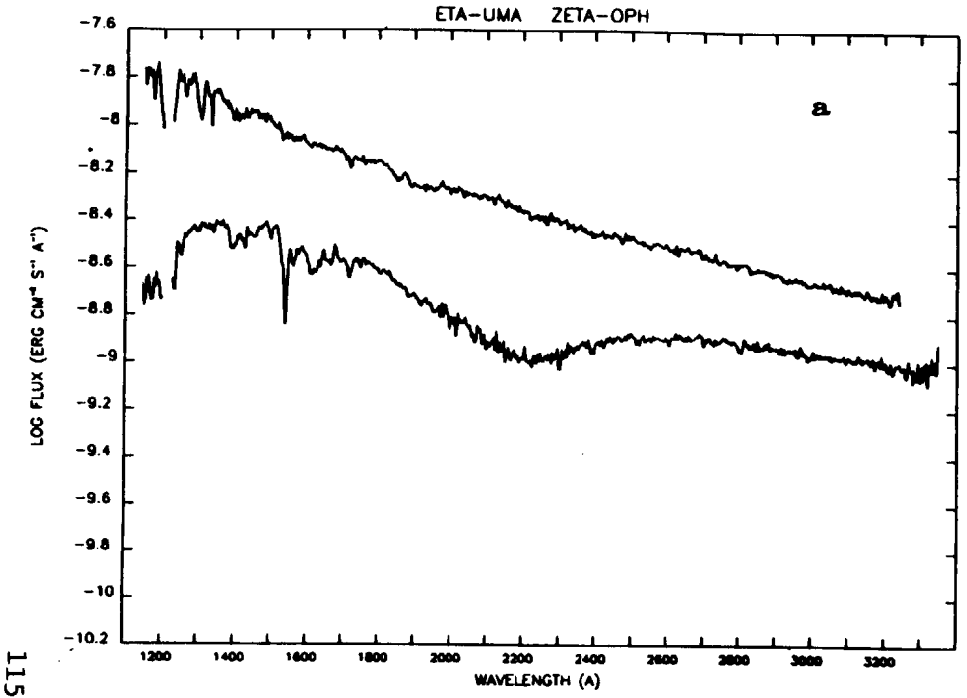
ETA-UMA ZETA-OPH
a
LOG FLUX (ERG CM⁻² S⁻¹ A⁻¹)
WAVELENGTH (A)

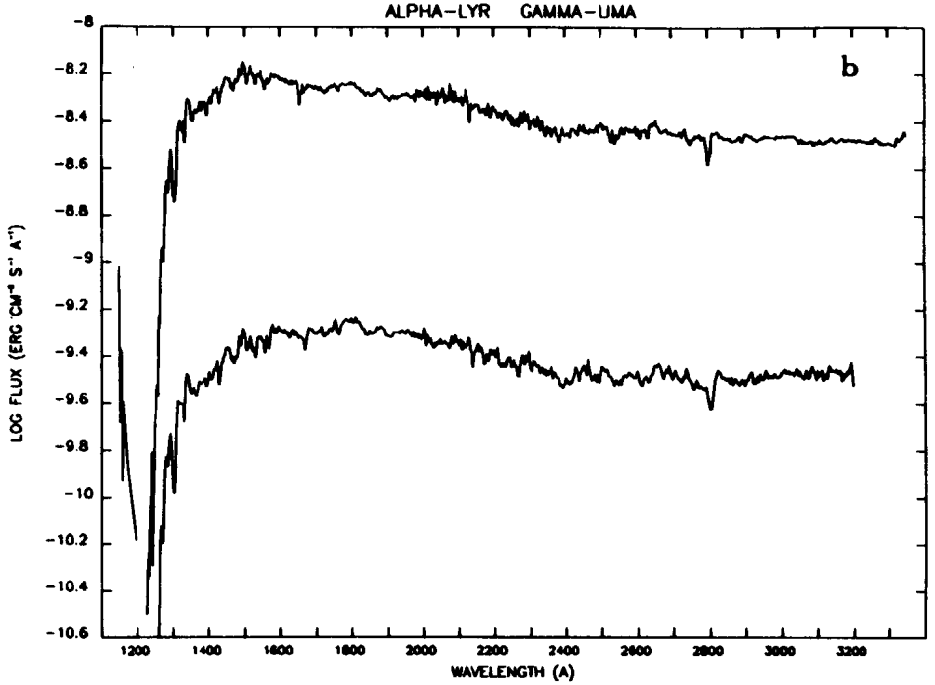
ALPHA-LYR GAMMA-UMA
b
LOG FLUX (ERG CM⁻² S⁻¹ A⁻¹)
WAVELENGTH (A)

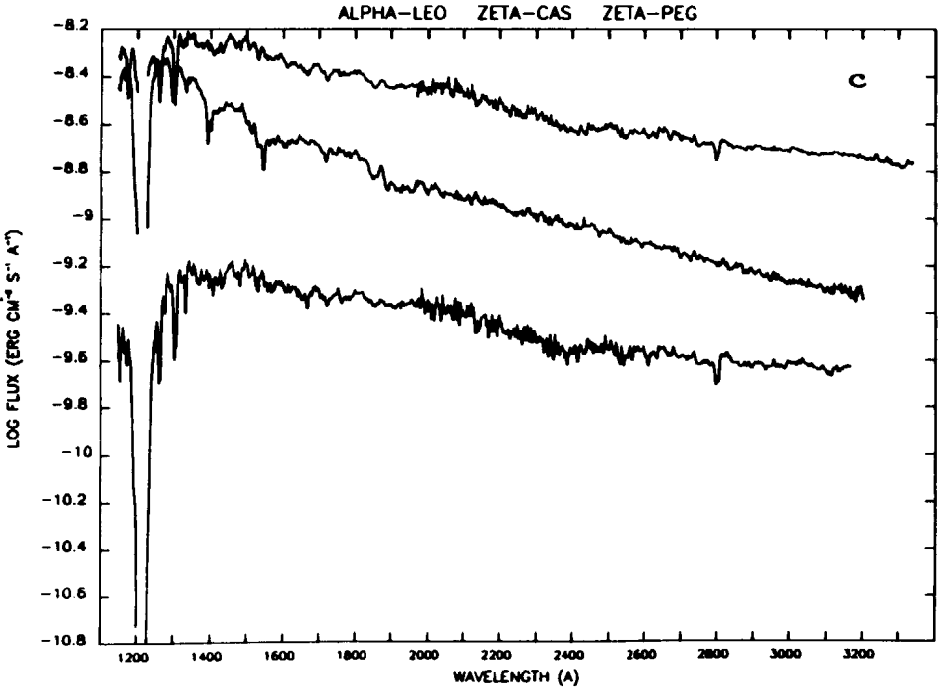
ALPHA-LEO ZETA-CAS ZETA-PEG
c
LOG FLUX (ERG CM⁻² S⁻¹ A⁻¹)
WAVELENGTH (A)

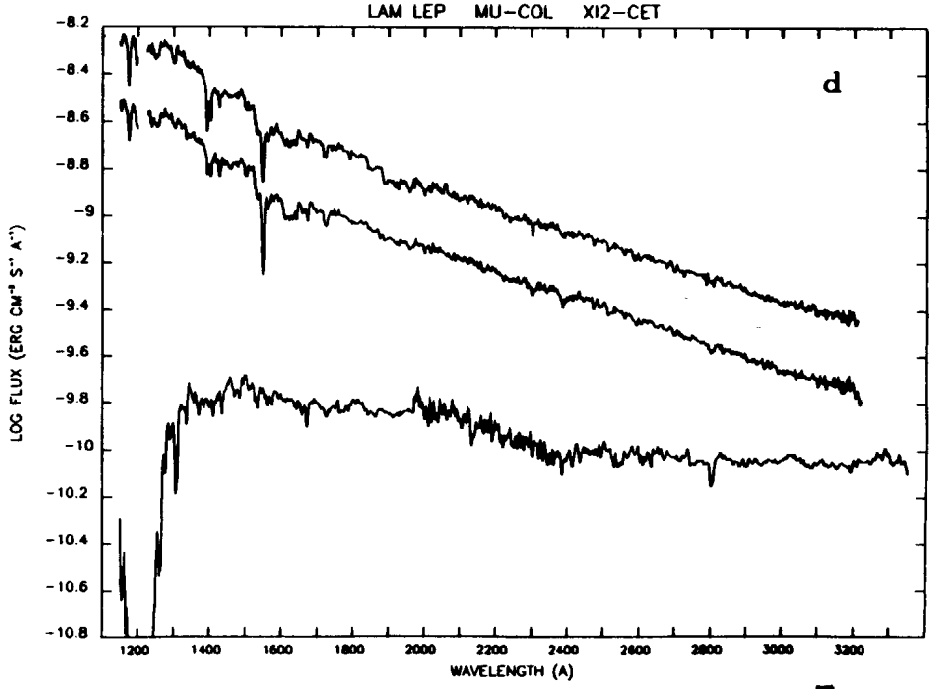
LAM LEP MU-COL XI2-CET
d
LOG FLUX (ERG CM⁻² S⁻¹ A⁻¹)
WAVELENGTH (A)

Fig. 3

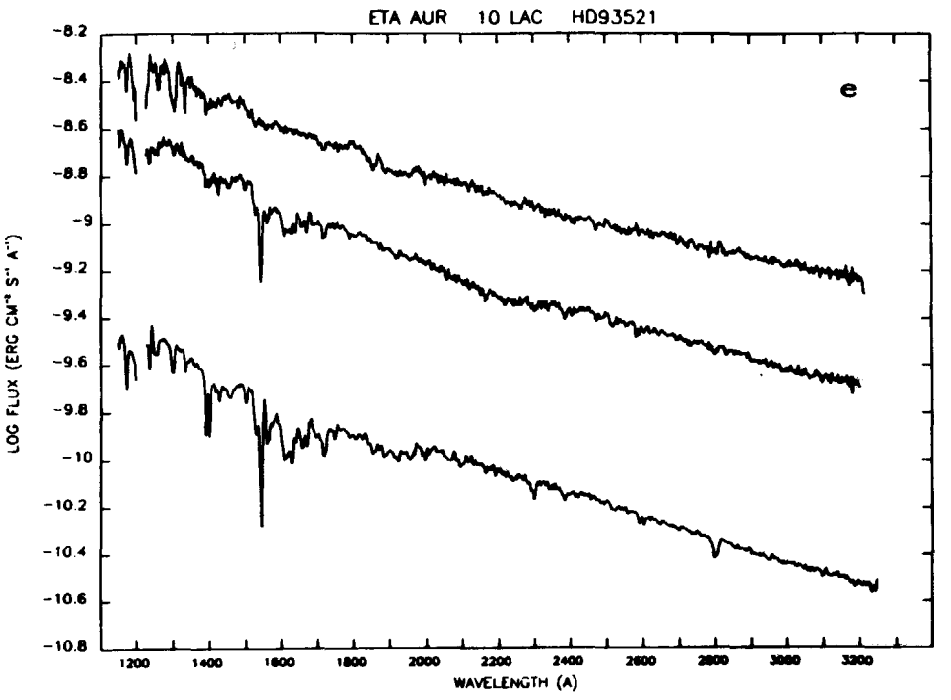
ETA AUR 10 LAC HD93521
e
LOG FLUX (ERG CM⁻² S⁻¹ A⁻¹)
WAVELENGTH (A)

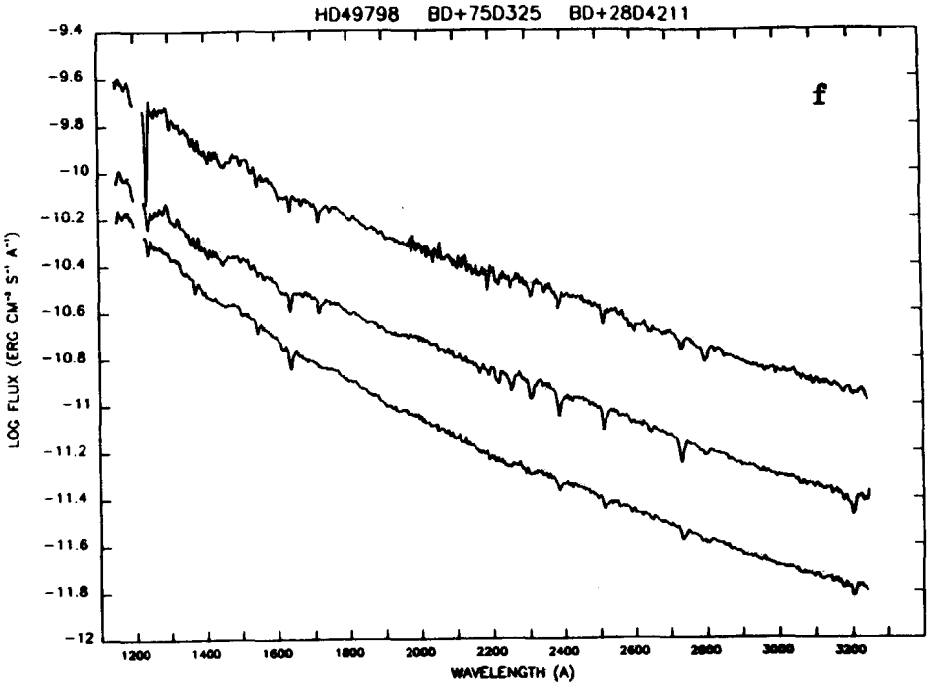
HD49798 BD+75D325 BD+28D4211
f
LOG FLUX (ERG CM⁻² S⁻¹ A⁻¹)
WAVELENGTH (A)

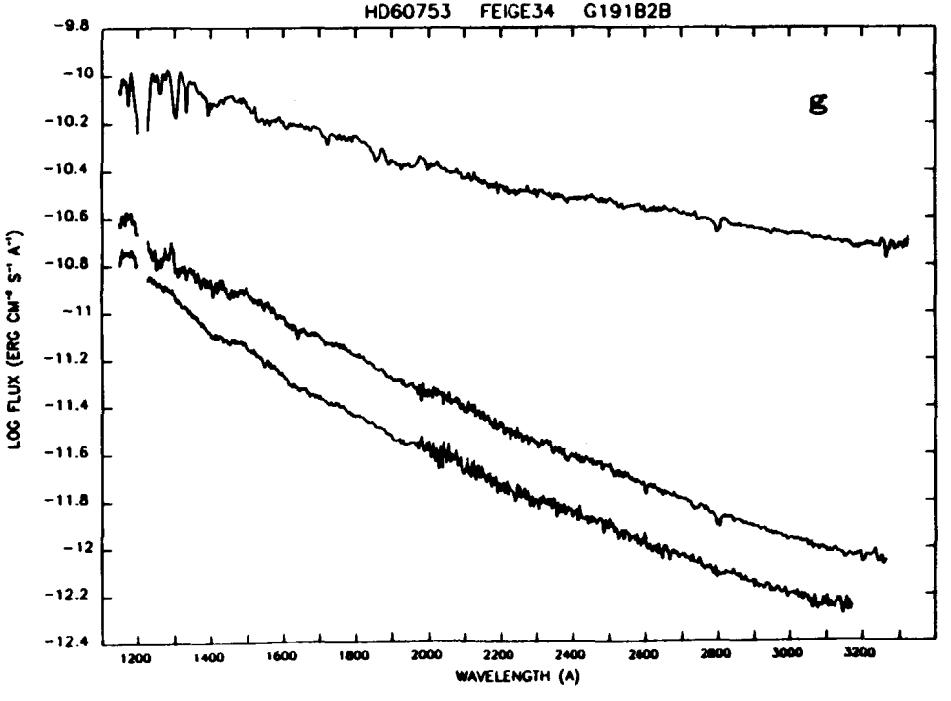
HD60753 FEIGE34 G191B2B
g
LOG FLUX (ERG CM⁻² S⁻¹ A⁻¹)
WAVELENGTH (A)

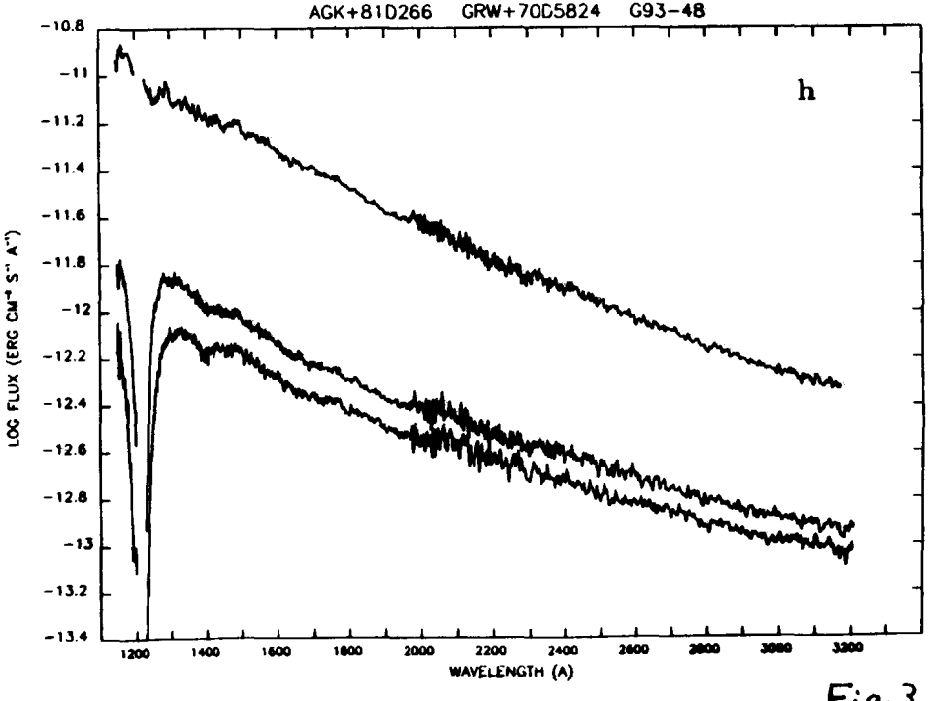
AGK+81D266 GRW+70D5824 G93-48
h
LOG FLUX (ERG CM⁻² S⁻¹ A⁻¹)
WAVELENGTH (A)

Fig. 3

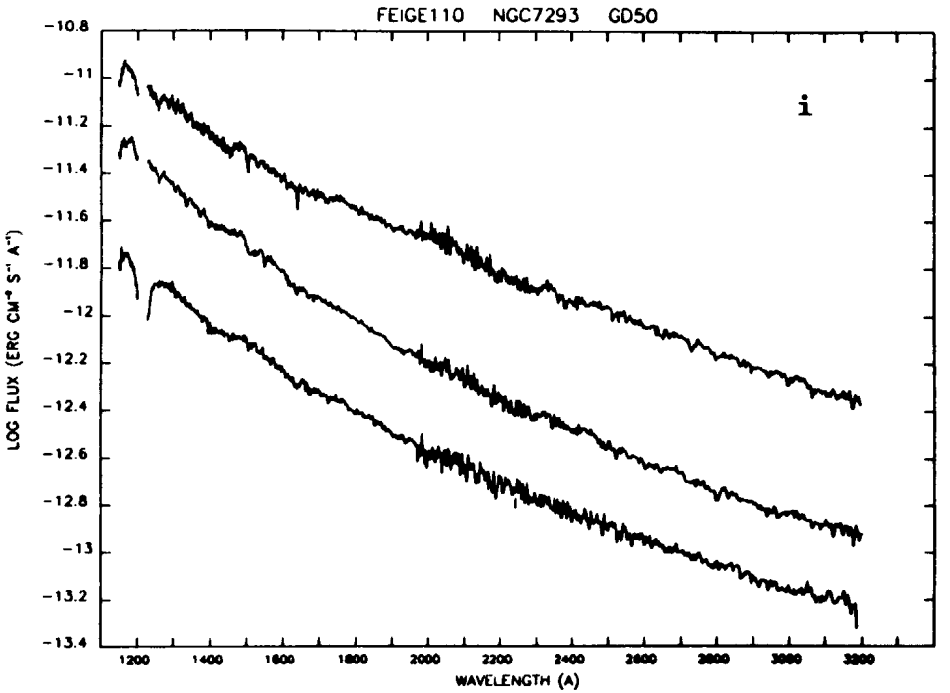
FEIGE110 NGC7293 GD50
i
LOG FLUX (ERG CM⁻² S⁻¹ A⁻¹)
WAVELENGTH (A)

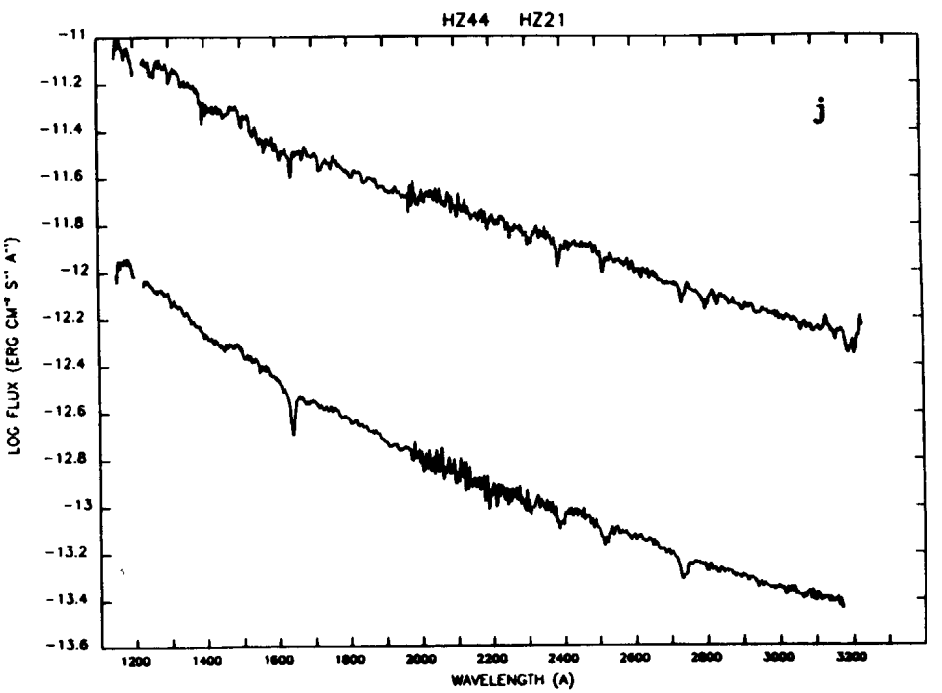
HZ44 HZ21
j
LOG FLUX (ERG CM⁻² S⁻¹ A⁻¹)
WAVELENGTH (A)

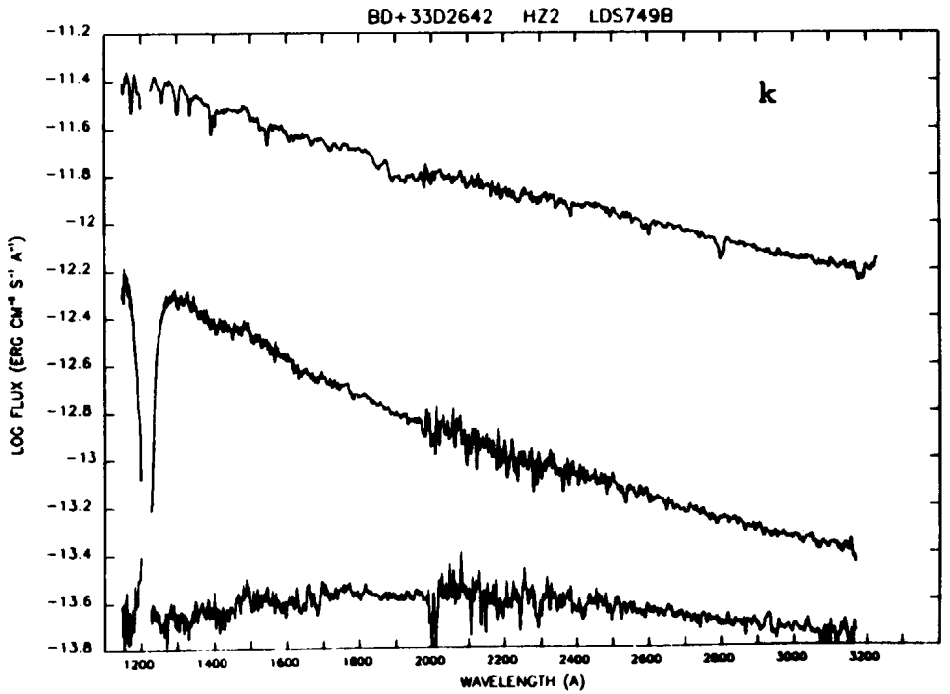
BD+33D2642 HZ2 LDS749B
k
LOG FLUX (ERG CM⁻² S⁻¹ A⁻¹)
WAVELENGTH (A)

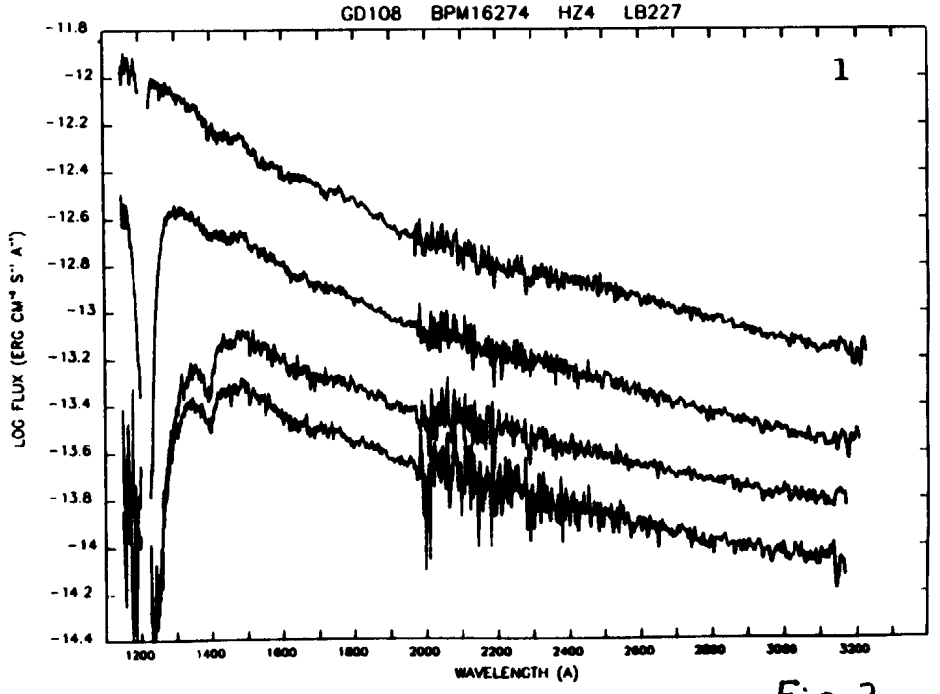
GD108 BPM16274 HZ4 LB227
l
LOG FLUX (ERG CM⁻² S⁻¹ A⁻¹)
WAVELENGTH (A)

Fig. 3

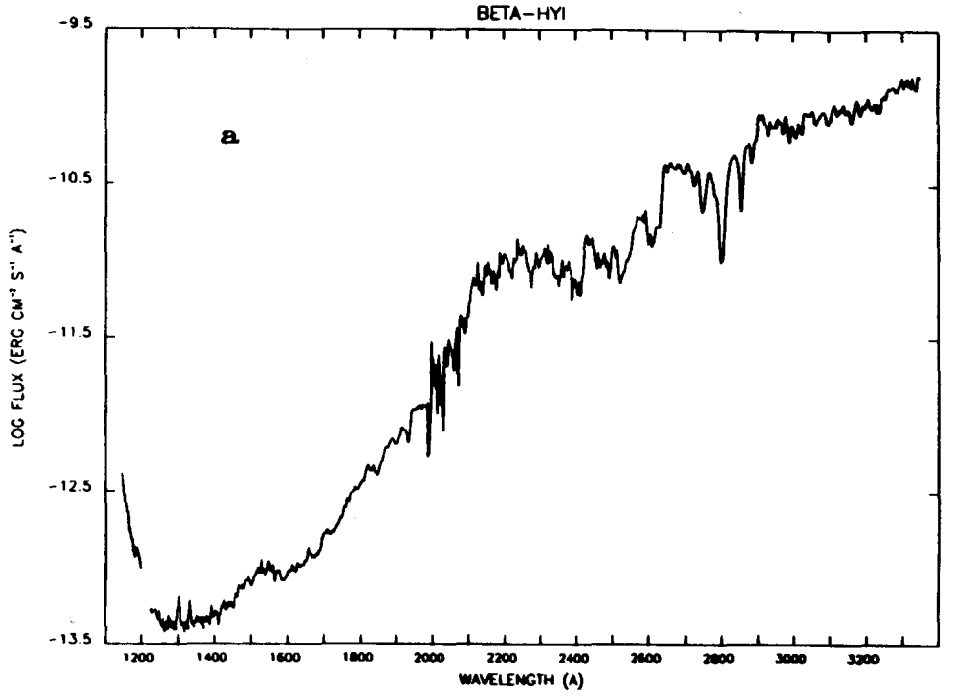
BETA-HYI
a
LOG FLUX (ERG CM⁻² S⁻¹ A⁻¹)
WAVELENGTH (A)

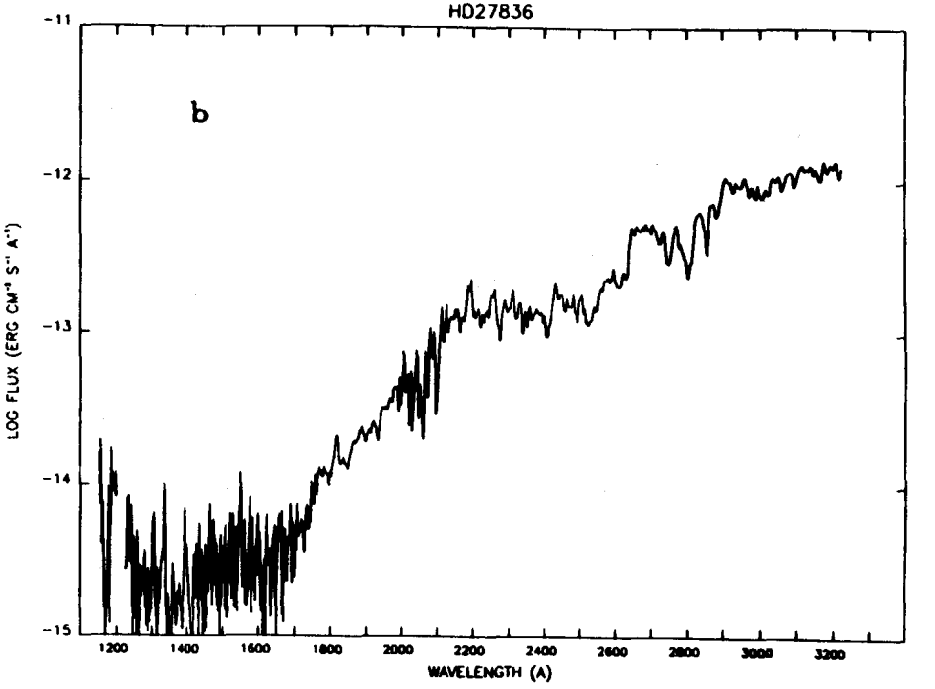
HD27836
b
LOG FLUX (ERG CM⁻² S⁻¹ A⁻¹)
WAVELENGTH (A)

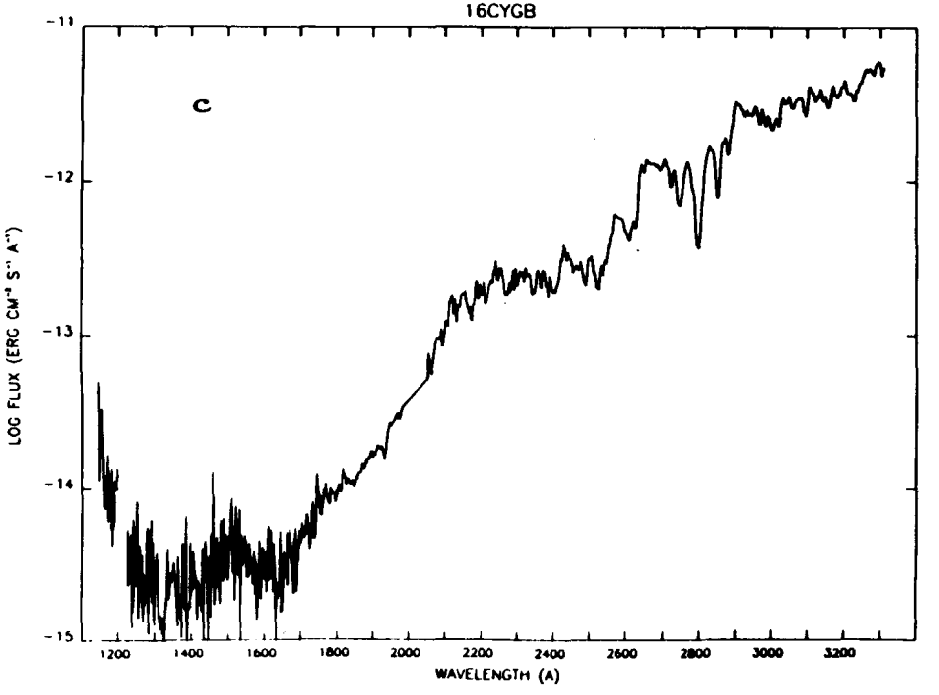
16CYGB
c
LOG FLUX (ERG CM⁻² S⁻¹ A⁻¹)
WAVELENGTH (A)

Fig. 4

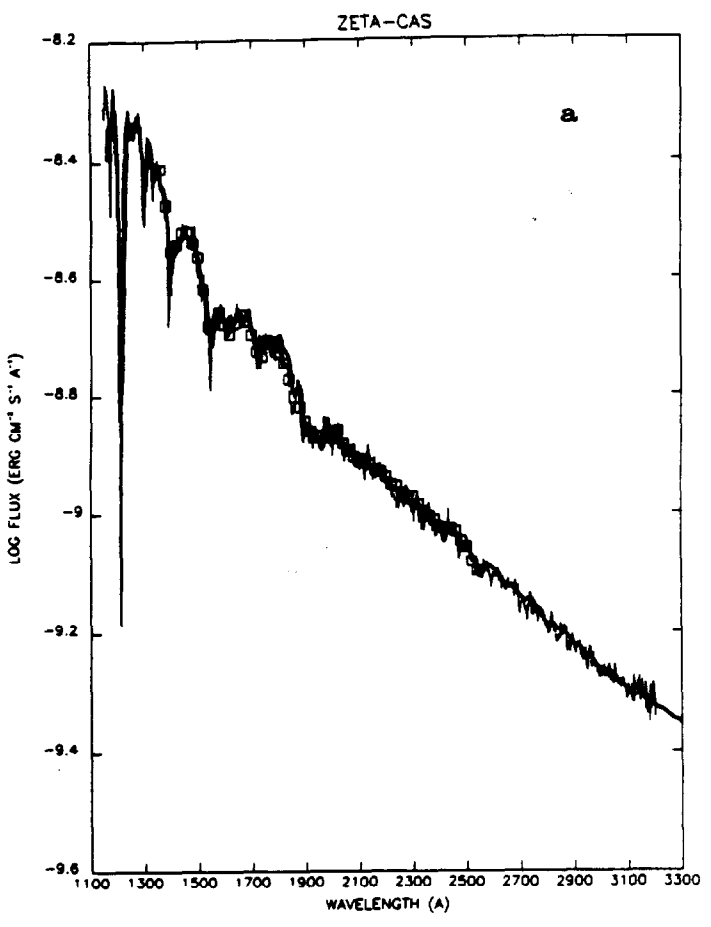
ZETA-CAS
a
LOG FLUX (ERG CM⁻² S⁻¹ A⁻¹)
WAVELENGTH (A)

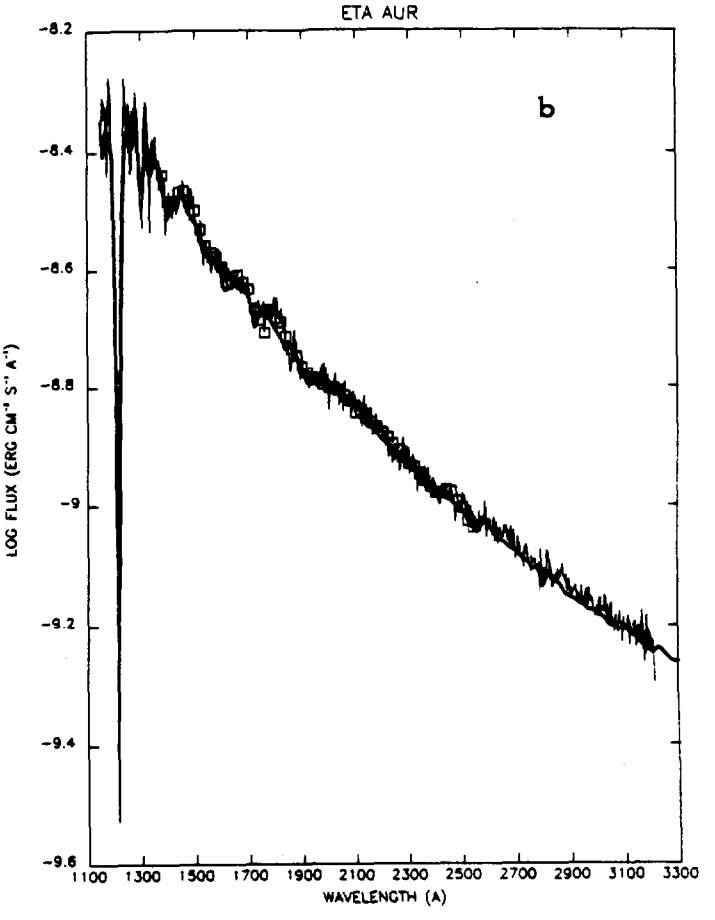
ETA AUR
b
LOG FLUX (ERG CM⁻² S⁻¹ A⁻¹)
WAVELENGTH (A)

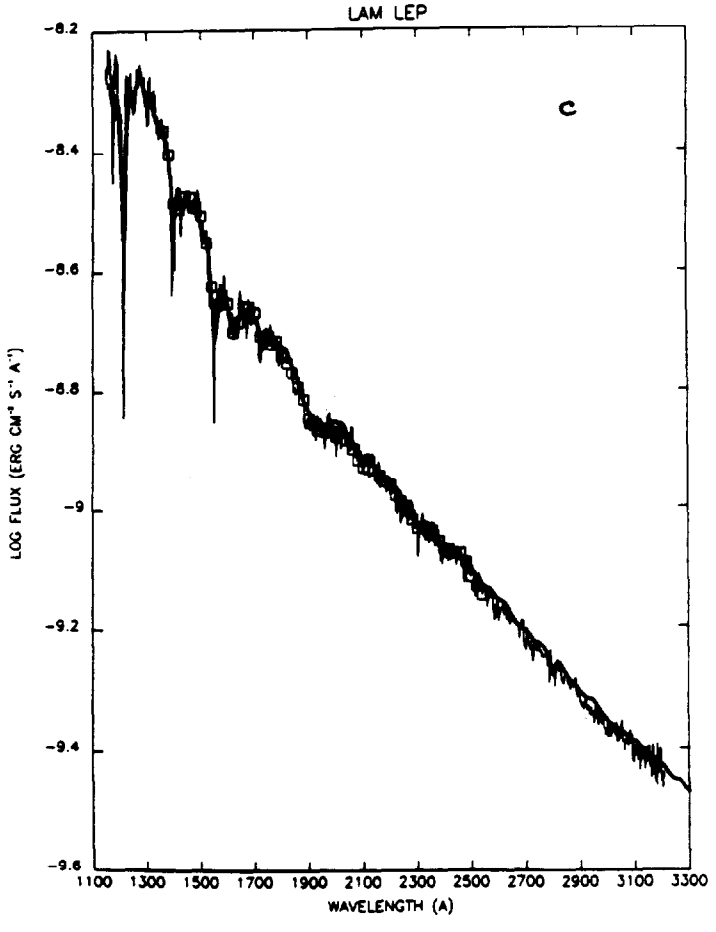
LAM LEP
c
LOG FLUX (ERG CM⁻² S⁻¹ A⁻¹)
WAVELENGTH (A)

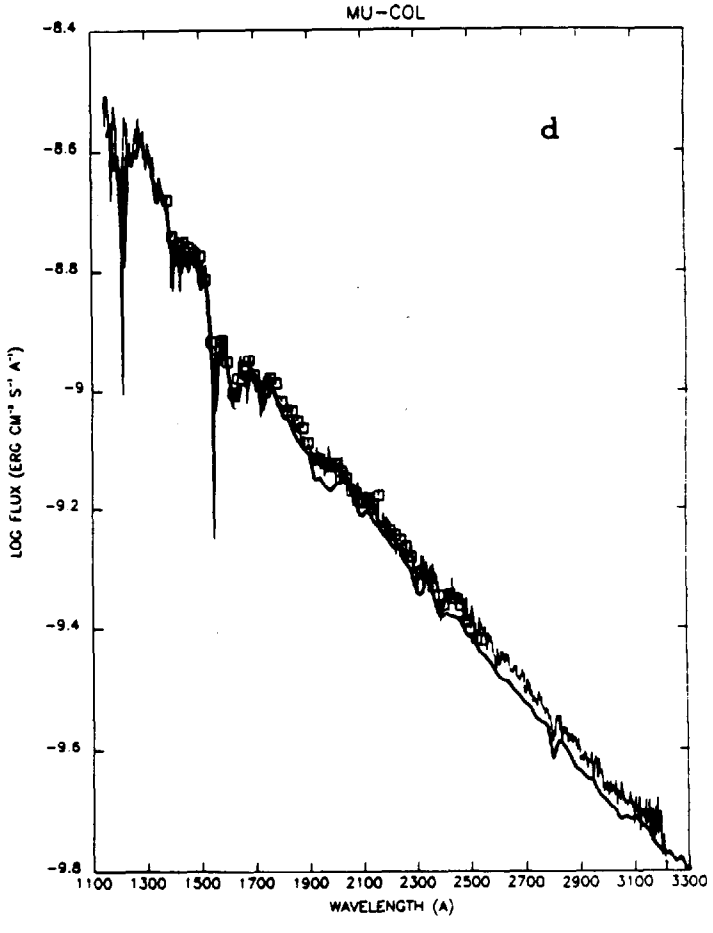
MU-COL
d
LOG FLUX (ERG CM⁻² S⁻¹ A⁻¹)
WAVELENGTH (A)

Fig. 5

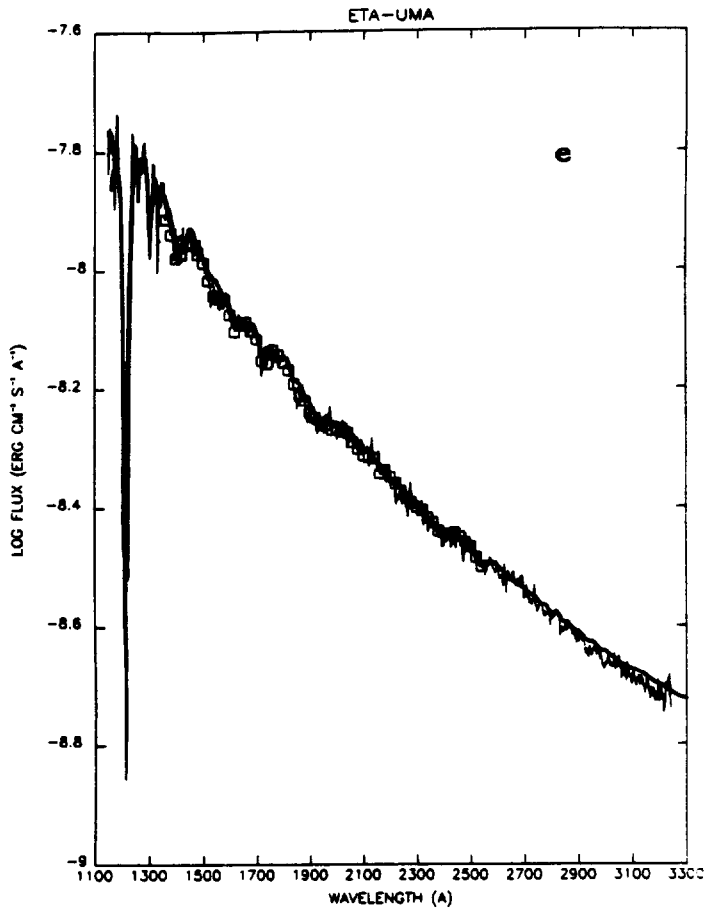
ETA-UMA
e
LOG FLUX (ERG CM⁻² S⁻¹ A⁻¹)
WAVELENGTH (A)

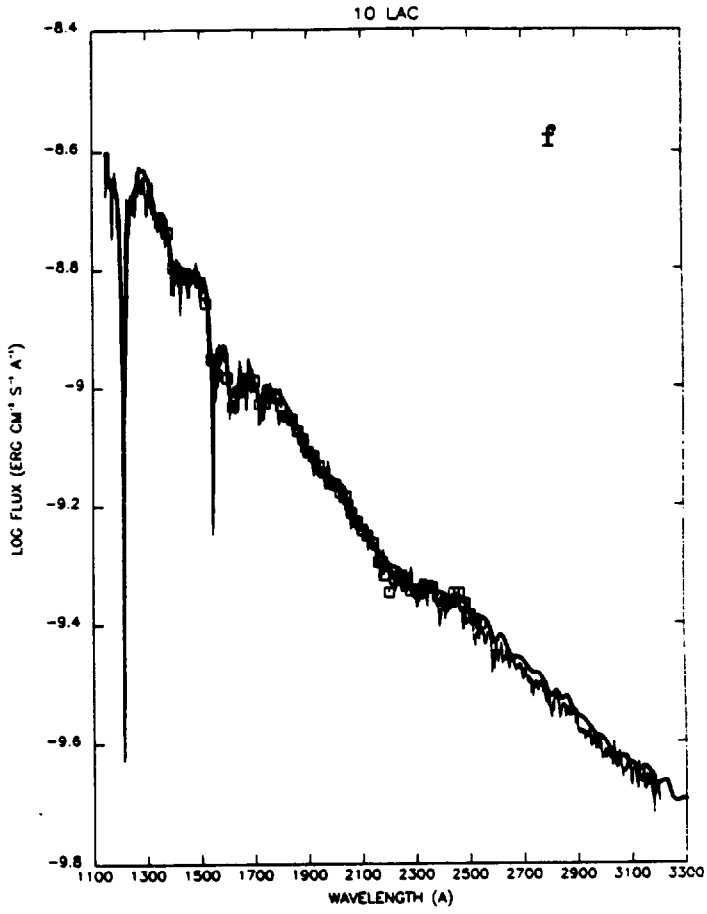
10 LAC
f
LOG FLUX (ERG CM⁻² S⁻¹ A⁻¹)
WAVELENGTH (A)

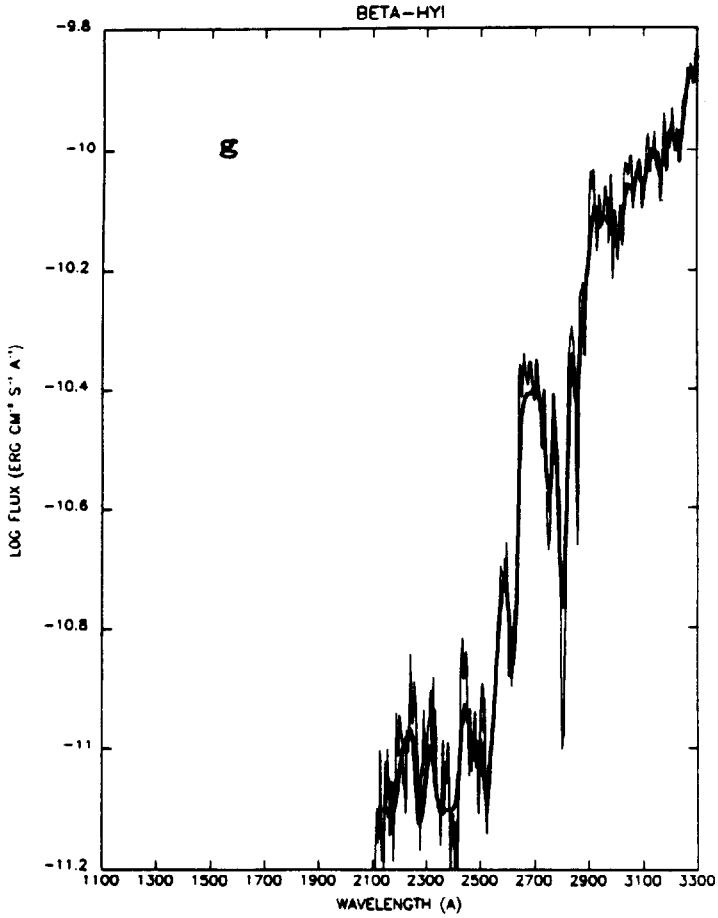
BETA-HYI
g
LOG FLUX (ERG CM⁻² S⁻¹ A⁻¹)
WAVELENGTH (A)

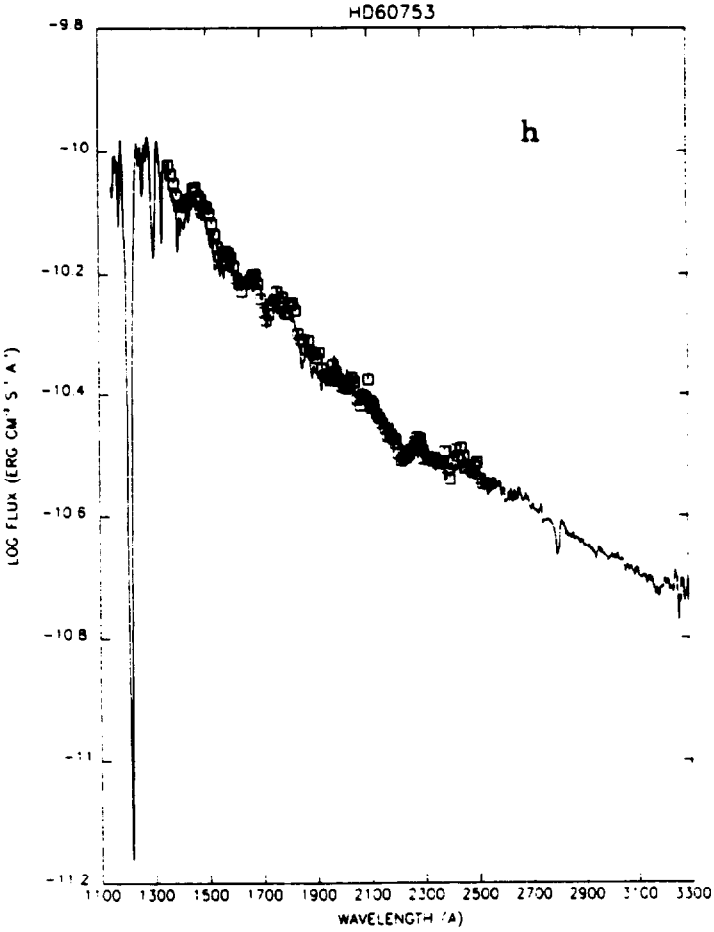
HD60753
h
LOG FLUX (ERG CM⁻² S⁻¹ A⁻¹)
WAVELENGTH (A)

Fig. 5

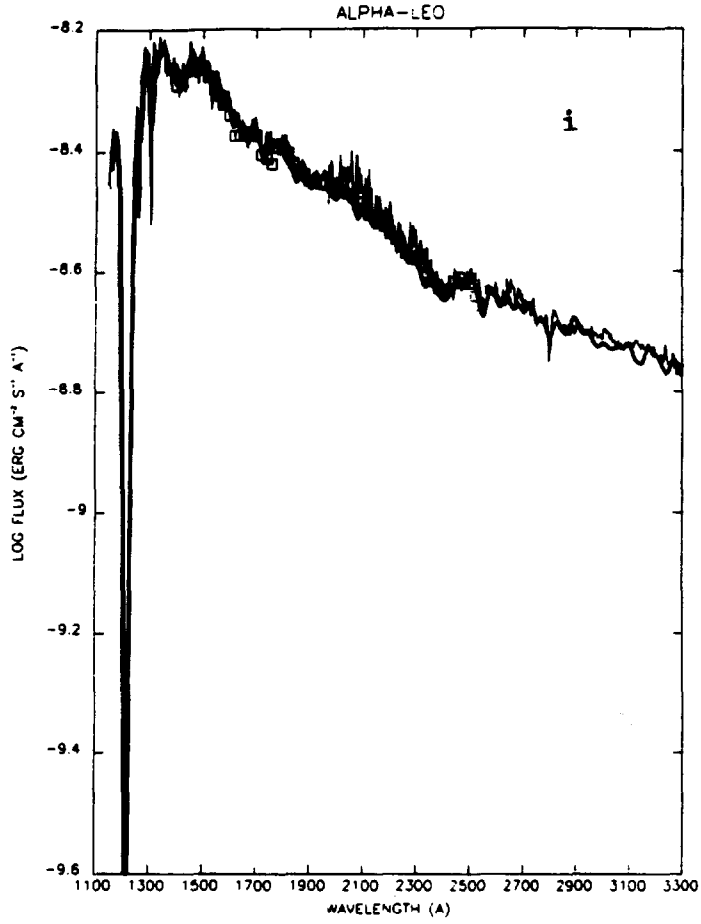
ALPHA-LEO
i
LOG FLUX (ERG CM⁻² S⁻¹ A⁻¹)
WAVELENGTH (A)

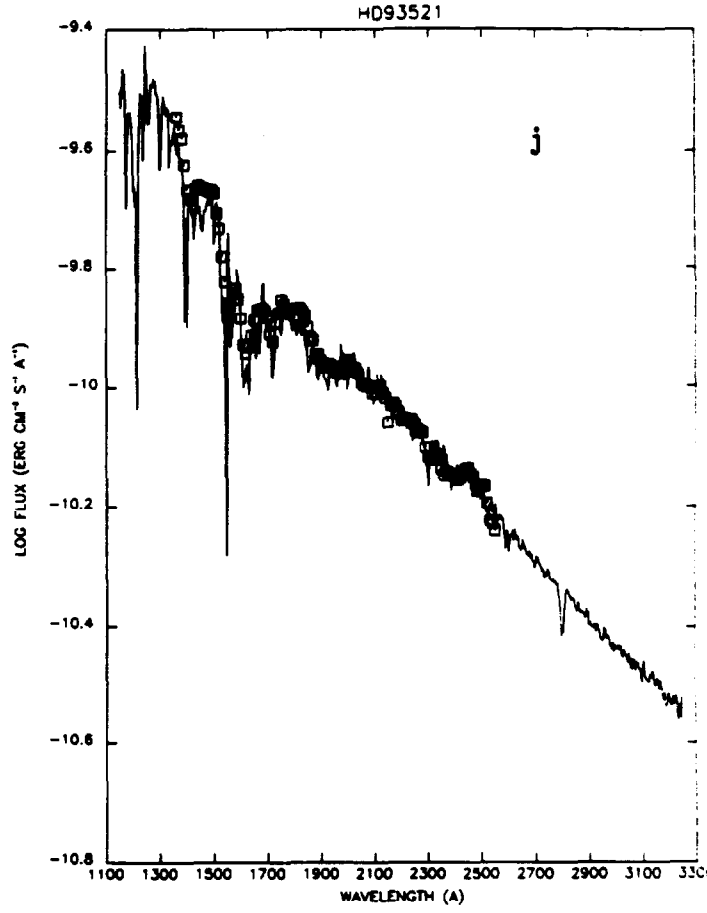
HD93521
j
LOG FLUX (ERG CM⁻² S⁻¹ A⁻¹)
WAVELENGTH (A)

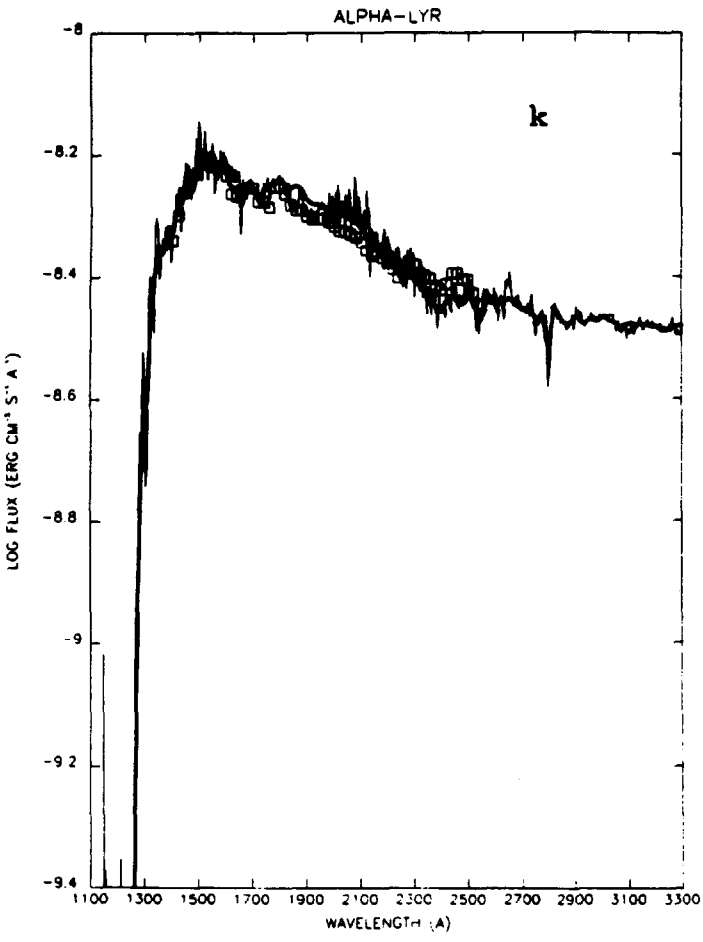
ALPHA-LYR
k
LOG FLUX (ERG CM⁻² S⁻¹ A⁻¹)
WAVELENGTH (A)

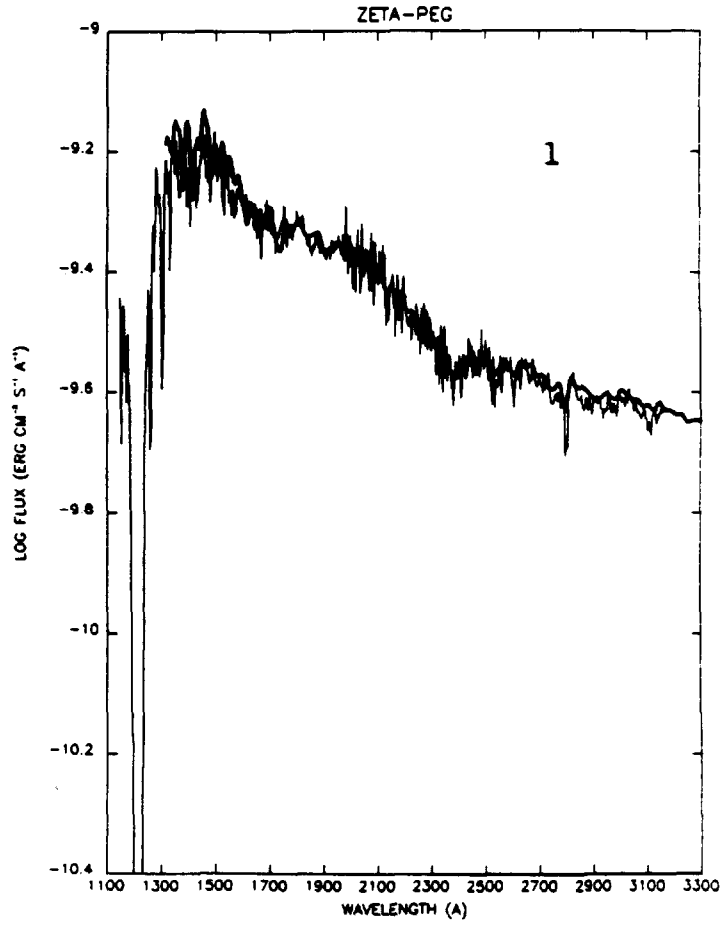
ZETA-PEG
l
LOG FLUX (ERG CM⁻² S⁻¹ A⁻¹)
WAVELENGTH (A)

Fig. 5

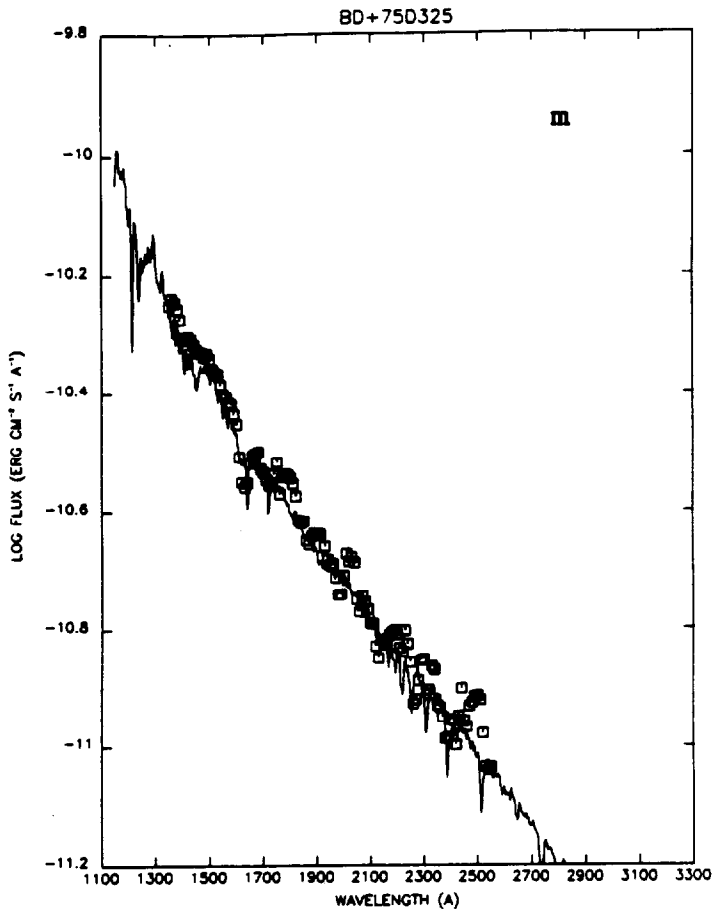
BD+75D325
m
LOG FLUX (ERG CM⁻² S⁻¹ A⁻¹)
WAVELENGTH (A)

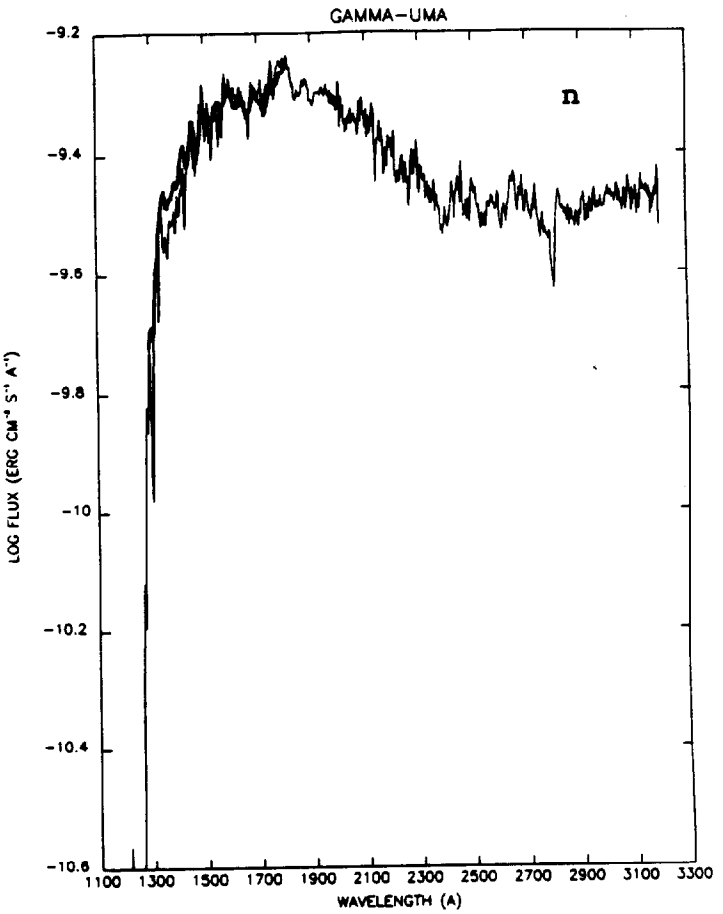
GAMMA-UMA
n
LOG FLUX (ERG CM⁻² S⁻¹ A⁻¹)
WAVELENGTH (A)

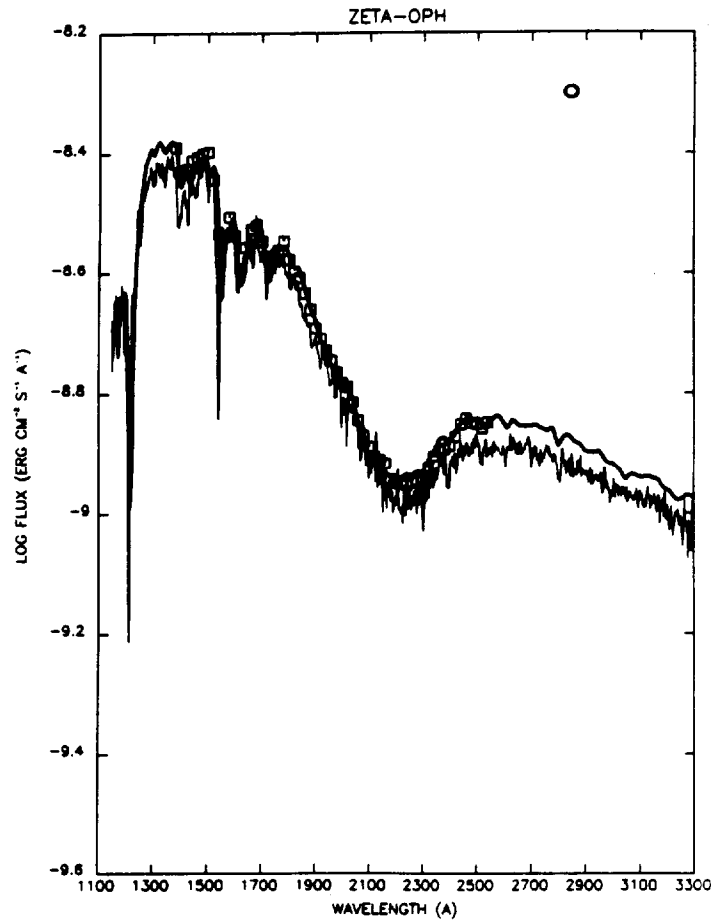
ZETA-OPH
o
LOG FLUX (ERG CM⁻² S⁻¹ A⁻¹)
WAVELENGTH (A)

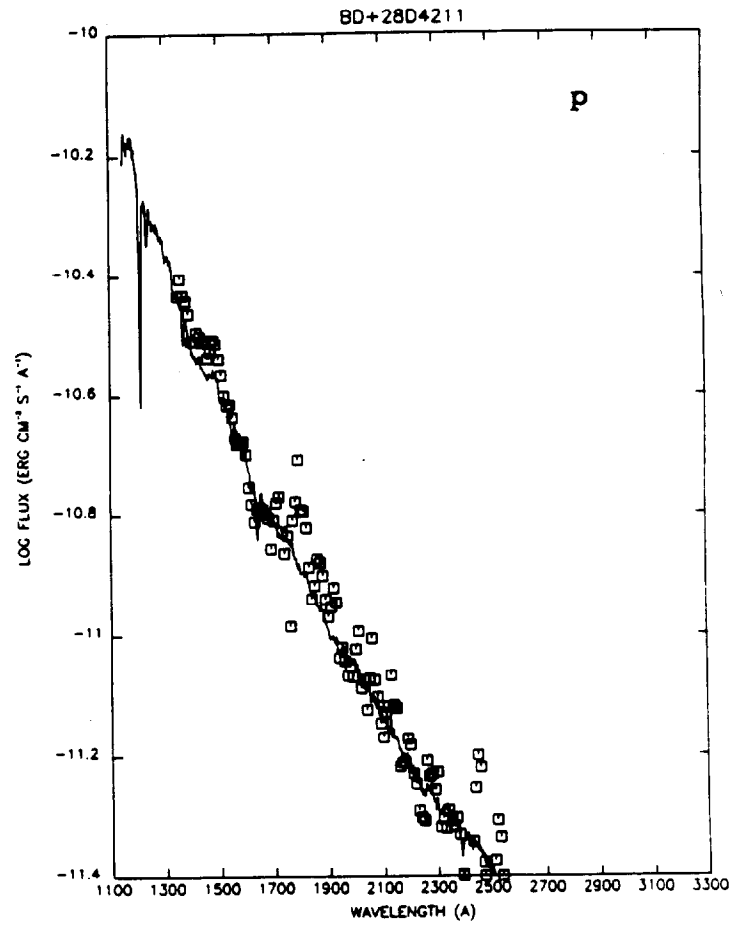
BD+28D4211
p
LOG FLUX (ERG CM⁻² S⁻¹ A⁻¹)
WAVELENGTH (A)

Fig. 5

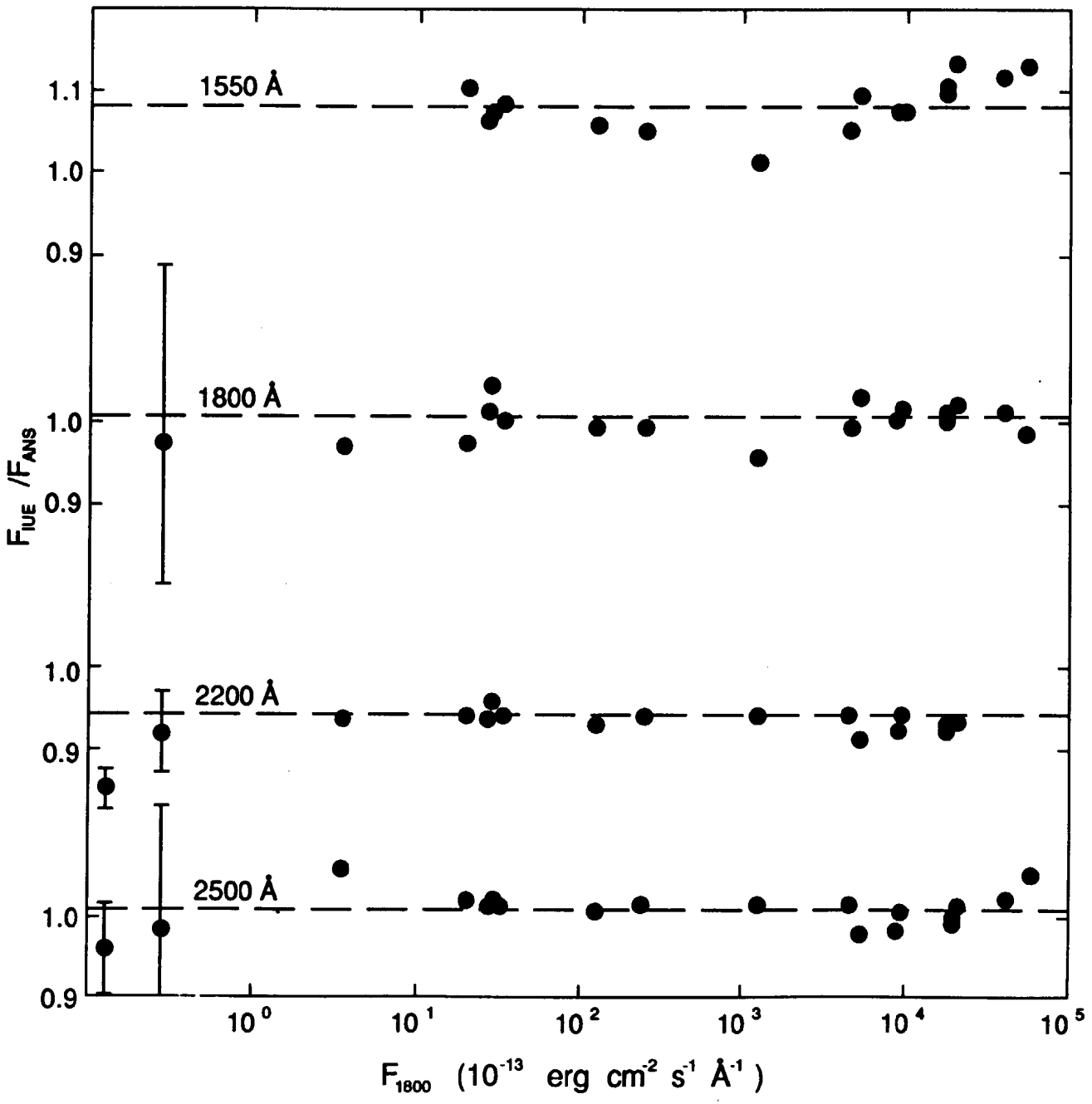
1550 Å
1800 Å
2200 Å
2500 Å
1.1
1.0
0.9
1.0
0.9
1.0
0.9
1.0
0.9
F_{IUE}/F_{ANS}
10^0
10^1
10^2
10^3
10^4
10^5
F_{1800} (10^{-13} erg cm^{-2} s^{-1} Å^{-1})

Fig. 6

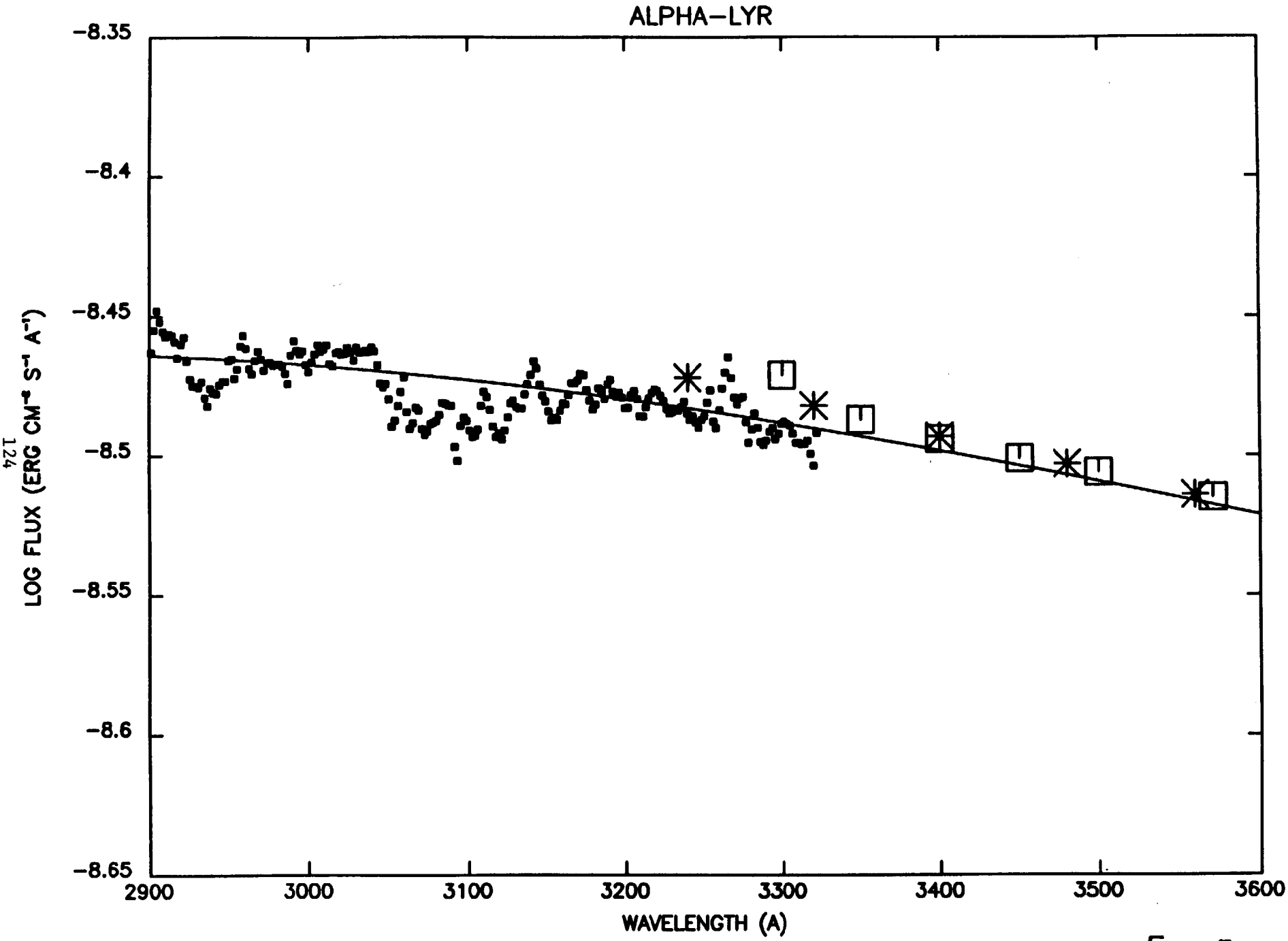
ALPHA–LYR
LOG FLUX (ERG CM⁻² S⁻¹ A⁻¹)
WAVELENGTH (A)
-8.35
-8.4
-8.45
-8.5
-8.55
-8.6
-8.65
2900
3000
3100
3200
3300
3400
3500
3600

Fig. 7

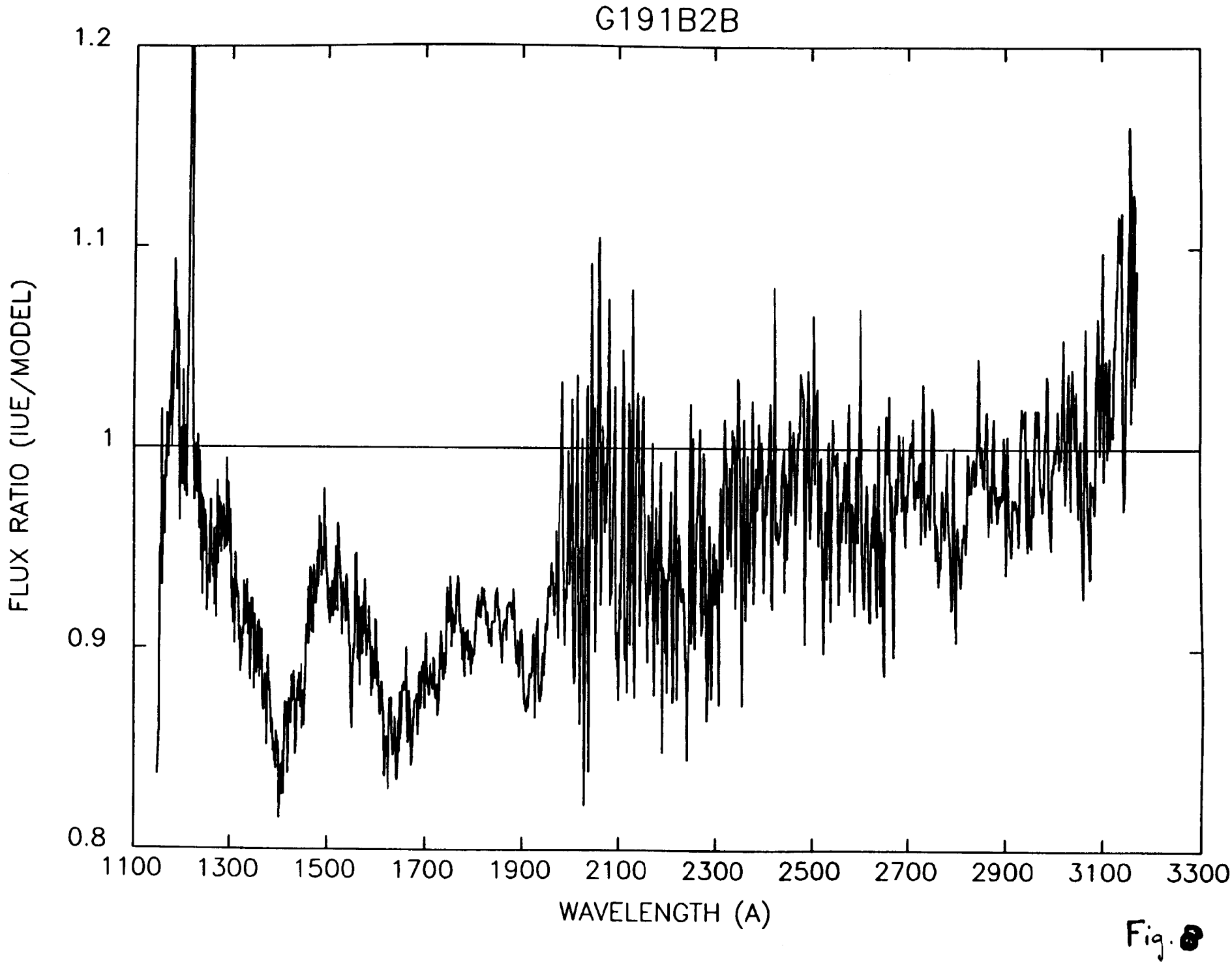
G191B2B
1.2
1.1
1
0.9
0.8
FLUX RATIO (IUE/MODEL)
1100
1300
1500
1700
1900
2100
2300
2500
2700
2900
3100
3300
WAVELENGTH (A)

Fig. 8